Tumor Stroma-Derived TGF-β Limits Myc-Driven Lymphomagenesis *via* Suv39h1-Dependent Senescence

AUTHORS/AFFILIATIONS

Maurice Reimann[1,6], Soyoung Lee[1,2,6], Christoph Loddenkemper[3,6], Jan R. Dörr[1,6], Vedrana Tabor[2,6], Peter Aichele[4], Harald Stein[3], Bernd Dörken[1,2], Thomas Jenuwein[5], and Clemens A. Schmitt[1,2]

[1]Charité - Universitätsmedizin Berlin/Molekulares Krebsforschungszentrum der Charité - MKFZ, Berlin, Germany

[2]Max-Delbrück-Center for Molecular Medicine, Berlin, Germany

[3]Charité - Universitätsmedizin Berlin/Department of Pathology, Campus Benjamin Franklin, Berlin, Germany

[4]University Hospital Freiburg, Department of Immunology, 79104 Freiburg, Germany

[5]Research Institute of Molecular Pathology, Vienna, Austria (present address: Max-Planck-Institute of Immunology, Freiburg, Germany)

[6]These authors contributed equally to this work

Correspondence: clemens.schmitt@charite.de. Fon +49-30-450 553 687; Fax +49-30-450 553 986

RUNNING TITLE

Myc induces senescence *via* a DDR and stromal TGF-β

SUMMARY

Activated RAS/BRAF oncogenes induce cellular senescence as a tumor-suppressive barrier in early cancer development, at least in part, *via* an oncogene-evoked DNA damage response (DDR). In contrast, Myc activation – although producing a DDR as well – is known to primarily elicit an apoptotic countermeasure. Using the Eμ-*myc* transgenic mouse lymphoma model, we show here *in vivo* that apoptotic lymphoma cells activate macrophages to secrete transforming growth factor–β (TGF-β) as a critical non-cell-autonomous inducer of cellular senescence. Accordingly, neutralization of TGF-β action, like genetic inactivation of the senescence-related histone methyltransferase Suv39h1, significantly accelerates Myc-driven tumor development *via* cancellation of cellular senescence. These findings, recapitulated in human aggressive B-cell lymphomas, demonstrate that tumor-prompted stroma-derived signals may limit tumorigenesis by feedback senescence induction.

HIGHLIGHTS

- **Myc drives tumor-limiting senescence *via* cell-autonomous and non-cell-autonomous ways**
- **The histone methyltransferase Suv39h1 is essential for Myc-induced senescence**
- **Apoptotic body-engulfing macrophages secrete TGF-β that induces tumor senescence**
- **These tumor/host interactions were recapitulated in human aggressive B-cell lymphomas**

GRAPHICAL ABSTRACT

is enclosed.

SIGNIFICANCE

Cancer entities with constitutive Myc expression, among them aggressive B-cell lymphomas, typically display high levels of apoptosis. So far, cellular senescence as another oncogene-inducible safeguard program has been recognized in RAS/BRAF-driven scenarios, but not as a *bona fide* Myc-evoked anti-cancer mechanism. Utilizing the genetically tractable Eμ-*myc* transgenic mouse lymphoma model and presenting supportive evidence from human aggressive B-cell lymphoma samples, this study establishes a novel network of tumor/host immune cell interactions in which apoptotic tumor cells launch a paracrine response in non-malignant bystanders that limits lymphomagenesis by cellular senescence. Our data expand the relevance of oncogene-induced senescence to Myc-driven cancers, and highlight the tumor stroma as a critical contributor and potential therapeutic target in this process.

INTRODUCTION

Mitogenic oncogenes provoke checkpoint-mediated cellular countermeasures such as apoptosis or premature senescence, a terminal G1 arrest involving the p53 and $p16^{INK4a}$ tumor suppressors that is characterized by typical transcriptional, biochemical and morphological alterations (Campisi and d'Adda di Fagagna, 2007; Hemann and Narita, 2007). RAS- or BRAF-initiated senescent lesions *in vitro* and *in vivo* exhibit chromatin changes that include the transcriptionally repressive tri-methylation mark at H3K9 (H3K9me3) and focal enrichment of HP1 proteins for which H3K9me3 provides a docking site (Bartkova et al., 2006; Braig et al., 2005; Collado et al., 2005; Lachner et al., 2001; Michaloglou et al., 2005; Narita et al., 2003). Mechanistically, hypophosphorylated Retinoblastoma (Rb) protein, bound to growth-promoting E2F transcription factors, may recruit H3K9 methyltransferase activities such as Suv39h1 to direct heterochromatinization to the vicinity of E2F-responsive promoters, thus silencing S-phase genes (Narita et al., 2003). Increasing evidence points towards an oncogene-induced DDR as critical upstream trigger of the senescence program (Bartkova et al., 2006; Di Micco et al., 2006; Mallette et al., 2007). Indeed, Myc and RAS oncogenes cause DNA damage by inducing reactive oxygen species (ROS) and generating stalled DNA replication intermediates (Di Micco et al., 2006; Lee et al., 1999; Reimann et al., 2007; Vafa et al., 2002). However, both prototypic oncogenes produce very different outcomes – *i.e.* predominantly cellular senescence following RAS/BRAF and apoptosis in response to Myc activation – when activated in primary cells *in vitro* (Evan et al., 1992; Serrano et al., 1997).

So far, there has been no clear evidence that Myc induction in primary cells may cause senescence under physiological conditions *in vitro* or *in vivo* (Feldser and Greider, 2007; Grandori et al., 2003; Guney et al., 2006). One cell-autonomous explanation for Myc's primarily pro-apoptotic action might be that Myc favors

apoptosis over arrest by influencing p53-dependent transactivation processes in response to DNA damage (Seoane et al., 2002).

The purpose of this study was to determine the contribution of cellular senescence as a tumor-suppressive mechanism in a transgenic mouse model of Myc-driven lymphomagenesis reminiscent of aggressive B-cell lymphomas in humans. Given the well-established predominantly apoptotic response to Myc activation in primary cells *in vitro*, we specifically aimed to dissect cell-autonomous and non-cell-autonomous components of Myc-related senescence *in vivo*.

RESULTS

Suv39h1-Dependent Cellular Senescence Limits Myc-Induced Lymphomagenesis

To determine the role of cellular senescence in Myc-driven tumorigenesis, we studied the impact of senescence-compromising Suv39h1 loss in Eμ-*myc* transgenic mice (Adams et al., 1985; Braig et al., 2005), where genetic disruption of apoptosis strongly promotes B-cell lymphomagenesis (Egle et al., 2004; Schmitt et al., 2002b; Strasser et al., 1990). Mice that lacked one or both *Suv39h1* alleles developed lymphomas significantly faster than mice without a targeted defect at the *Suv39h1* locus ($P < 0.0001$ for either comparison, Figure 1A). Moreover, lymphomas that formed in *Suv39h1*$^{+/-}$ female mice invariably lost expression of the X-chromosomally encoded *Suv39h1* transcript, thereby explaining the indistinguishable tumor onset in *Suv39h1*$^{+/-}$ and *Suv39h1*$^{-}$ (*i.e. Suv39h1*$^{-/y}$ male and *Suv39h1*$^{-/-}$ female) mice (Figure 1A, insert). Importantly, the frequency of apoptosis measured as TUNEL (terminal deoxynucleotidyl transferase dUTP nick end labeling) reactivity, a hallmark of Myc-driven lymphomas, was virtually identical in Suv39h1-deficient lymphomas when

compared to control lymphomas (*i.e.* those that arose in Eμ-*myc* mice without a targeted *Suv39h1* lesion; Figure 1B). Furthermore, control and Suv39h1-deficient lymphomas presented with indistinguishable gross pathology, formed at comparable stages of B-cell development, both expressed *Suv39h2* transcripts, and displayed similar near-normal chromosome counts, unlike the previously reported chromosome-missegregated B-cell lymphomas that form in the absence of both *Suv39h1* and *Suvh39h2* alleles in non-transgenic mice (Peters et al., 2001) (data not shown). Thus, neither compromised apoptosis nor overt aneuploidy account for the accelerated lymphoma onset in Suv39h1-deficient Eμ-*myc* mice.

To directly assess oncogene-induced senescence as a potential component of delayed lymphoma manifestation, senescence-associated β-galactosidase (SA-β-gal) activity (Dimri et al., 1995) was analyzed in Suv39h1-deficient and control lymphomas. Virtually none of the cells in the *Suv39h1*$^{-}$ lymphoma sections, but an average of about 14% of the control lymphoma cells stained, often in a focal pattern, positive for SA-β-gal ($P < 0.001$; Figure 1B and 1C; see Figure S1A and S1B for further evidence that senescent cells are indeed B-lymphoma cells). Moreover, co-analysis of the proliferation marker Ki67 or bromodeoxyuridine (BrdU) incorporation, indicating DNA synthesis, with SA-β-gal or H3K9me3 staining confirmed the growth-arrested nature of SA-β-gal- or H3K9me3-positive cells (Figure 1D). Immunoblot analyses of bulk lymph node lysates indicated no differences in the expression levels of Myc and the cell-cycle inhibitor $p21^{CIP1}$ between control and *Suv39h1*$^{-}$ lymphomas, while significant amounts of hypophosphorylated/G1-phase Rb and of H3K9me3 were only found in control lymphomas, which also displayed slightly reduced levels of the CDK4/6 inhibitor $p16^{INK4a}$ and the E2F target Cyclin A (Figure 1E). Other histone modifications such as H3K4me3, acetylated H3K9, H3K27me3, or H4K20me3 appeared globally unaffected by Suv39h1 status (data not shown), underscoring the specific role of the Suv39h1-mediated H3K9me3 mark in the senescence process. Moreover, spleen samples derived

from young, lymphoma-free Eμ-*myc* mice (termed 'pre-neoplastic', albeit consisting of Myc-overexpressing normal B-cells) as compared to spleen sections from non-transgenic mice exhibited signs of cellular senescence in a strictly Myc- and Suv39h1-dependent fashion, indicating that oncogene-related senescence may delay tumorigenesis already at a pre-malignant state (Figure S1C). Thus, aggressive Myc-driven lymphomas develop and manifest with a significant fraction of cells that lack any proliferative activity and display marks of cellular senescence.

All Myc-lymphomas developing in *Suv39h1*$^{+/-}$;*p53*$^{+/-}$ or *Suv39h1*$^{-}$;*p53*$^{+/-}$ backgrounds selected against the remaining *p53* wild-type allele (12/12 cases tested "p53-null"; Figure 1F), as known from lymphomas forming in Eμ-*myc*;*p53*$^{+/-}$ mice (Schmitt et al., 1999), and, thus, against p53-dependent apoptosis. *Suv39h1* RNA expression was mostly retained in *Suv39h1*$^{+/-}$;*p53*$^{+/-}$-derived lymphomas (7/9 cases tested; Figure 1F), indicating that p53 loss co-ablates an apoptosis-independent tumor-suppressive function otherwise governed by Suv39h1. Accordingly, additional inactivation of *Suv39h1* produced no further acceleration of Eμ-*myc* lymphomagenesis in a *p53*$^{+/-}$ background (data not shown). Notably, and different from p53-null lymphomas, DDR-defective *ATM*$^{-/-}$ lymphomas displayed only a partial reduction of the senescent fraction at manifestation (Figure 1G and Figure S1D, showing, in addition, control lymphoma-comparable senescence in p16^{INK4a}-deficient *INK4a*$^{-/-}$ and p21^{CIP1}-deficient *CIP1*$^{-/-}$ lymphomas, but compromised senescence in *ARF*$^{-/-}$ lymphomas). Taken together, Myc-induced senescence presents *in vivo* as a p53-, Suv39h1-, and partly ATM-dependent program that complements apoptosis as an anti-oncogenic safeguard mechanism in Eμ-*myc* lymphomagenesis.

Activated Myc Promotes ATM/p53-Dependent Senescence

Myc activation is known to produce marks of DNA damage *in vivo* (Reimann et al., 2007), at least in part *via* ROS, which may link Myc *via* a DDR to Suv39h1-dependent senescence. Notably, Suv39h1 had no impact on γ-H2AX-marked DNA lesions and the DDR signature in pre-neoplastic Eμ-*myc* transgenic B-cells, or in lymphoma cells exposed to γ-irradiation (Figure S2A-C). However, in contrast to wild-type B-cells, primary B-cells lacking the DDR mediators ATM or p53 largely failed – like Suv39h1-deficient B-cells – to senesce in response to acute Myc overexpression *in vitro* (Figure 2A). If senescence detected in control lymphomas *in situ* is initiated *via* a Myc-evoked DDR, then genetic or pharmacological interference with the DDR should impact on the senescence response. Comparable to the $ATM^{-/-}$ scenario (Figure 1G), exposure of Eμ-*myc* transgenic mice to the ROS scavenger N-acetyl-cysteine (NAC) or to the ATM/ATR inhibitor caffeine that both blunt an oncogene-evoked DDR *in vivo* (Bartkova et al., 2006; Reimann et al., 2007) resulted in a profound, albeit only partial reduction of senescent lymphoma cells *in situ* (Figure S2D-F, also showing that ROS levels are Myc- but not Suv39h1-dependent).

To directly address the cell-autonomous potential of Myc to drive senescence, we tested whether a conditional p53 moiety would suffice to convert constitutive Myc signaling into a robust senescence response in apoptosis-incapable cells. To this end, we employed Eμ-*myc* mice carrying a 4-OH-tamoxifen (4-OHT)-inducible $p53ER^{TAM}$ knock-in allele, encoding a p53-estrogen receptor fusion protein that is inactive in the absence of 4-OHT (Martins et al., 2006). Expectedly, Eμ-*myc*;$p53ER^{TAM/+}$ lymphomas that arose in the absence of 4-OHT typically selected against the remaining *p53* wild-type allele (termed $p53ER^{TAM/(-)}$; 5/5 cases tested [data not shown and (Martins et al., 2006)]), thereby generating p53-null lymphomas in which p53 activity is restorable upon provision of 4-OHT (Figure S2G). Constitutively Myc-expressing and *bcl2*-

transduced (and, thus, apoptosis-protected) lymphoma cells quantitatively entered senescence following exposure to 4-OHT *in vitro*, while non-transgenic, Bcl2-protected p53ER^{TAM}-expressing B-cells lacked such a response (Figure 2B). Similarly, senescence was strongly induced when mice harboring Eμ-*myc*;*p53ER*$^{TAM/(-)}$/*bcl2* lymphomas were exposed to tamoxifen *in vivo* (Figure 2C). Importantly, pharmacological scavenging of ROS or ablation of the DDR attenuated, and, when combined, almost completely blocked the senescence induction of Eμ-*myc*;*p53ER*$^{TAM/(-)}$/*bcl2* lymphoma cells in response to 4-OHT *in vitro* (Figure 2D). Thus, acute overexpression of Myc in primary cells or p53 reactivation in the presence of constitutive Myc signaling unmasks the cell-autonomous, DDR-mediated pro-senescent capability of Myc.

TGF-β Induces Senescence of Myc-Driven Lymphoma Cells

Because neither ATM deficiency nor pharmacological DDR ablation was sufficient to fully abrogate senescence of Myc-driven lymphoma cells *in vivo*, we aimed to identify an additional stimulus that may complement oncogene-induced DDR signaling *in vivo*. Genome-wide transcriptional profiling of whole lymph node RNA preparations from Suv39h1-proficient *vs.* Suv39h1-deficient Eμ-*myc* lymphomas identified *TGF-β-induced gene* (Tgfbi; also known as Big-h3, β-ig H3, or keratoepithelin) as the most strongly differentially upregulated transcript. *Tgfbi*, a TGF-β target, was expressed 3.9-fold higher in *Suv39h1*$^{-}$ lymphomas, and encodes a secreted protein with cytostatic potential that was previously linked to cellular senescence (Dokmanovic et al., 2002) (see "Experimental Procedures" section for details and the confirmatory quantitative RT-PCR [RQ-PCR] analysis in Figure S3A). We found TGF-β1, known to induce cellular senescence in fibroblasts (Lin et al., 2004), to be detectable

in a multi-focal pattern in lymphoma sections reminiscent of the distribution of SA-β-gal-positive cells in control lymphomas (Figure 3A, compare to Figure 1B). Importantly, co-staining for the proliferation marker Ki67 unveiled that in areas with abundant TGF-β1 significantly less control cells were Ki67-positive when compared to *Suv39h1*$^{-}$ lymphomas (Figure 3A). Thus, TGF-β correlates with a cytostatic response selectively detectable in control lymphomas, and high *Tgfbi* levels in *Suv39h1*$^{-}$ cells are suggestive for a downstream defect in a TGF-β-inducible senescence program.

We sought to directly test the potential of exogenous TGF-β1 to induce cellular senescence in a Suv39h1-dependent fashion in Myc-driven lymphoma cells that were stably *bcl2*-transduced to block apoptosis. TGF-β1 countered proliferation in a dose-dependent manner and led to a complete growth arrest with features of cellular senescence, *i.e.* SA-β-gal activity and H3K9me3 expression, in control, but not in *Suv39h1*$^{-}$ lymphoma cells whose growth behavior remained largely unaffected by TGF-β1 treatment (Figure 3B). Lack of a cytostatic response in *Suv39h1*$^{-}$ cells was not due to a primary defect in TGF-β receptor signaling, since lymphoma cells of both genotypes exhibited phosphorylation of the intracellular TGF-β1 mediators Smad2 and Smad3 following TGF-β1 treatment *in vitro* (Figure S3B). In line with the transcriptionally repressive H3K9me3 mark selectively induced in control lymphomas (Figure 3B), TGF-β1-treated control lymphomas displayed reduced transcript levels of numerous E2F target genes, including *MCM7* or *Cyclin A* by microarray analysis, as well as increased levels of transcripts that encode for components of the heterochromatinization machinery such as *DNA methyltransferase 3B* or *HP1β* (Figure S3C, and Figure 3C for Cyclin A protein expression). The mechanism by which TGF-β utilizes Suv39h1, presumably in conjunction with Rb/E2F complexes (Laiho et al., 1990; Schwarz et al., 1995; Spender and Inman, 2009), to induce senescence appears to be indirect, since we were unable to detect a physical interaction between Suv39h1 and Smad proteins (Figure S3D). TGF-β1 was incapable of inducing $p15^{INK4b}$ or $p21^{CIP1}$ mRNA and

protein expression in lymphomas independent of their Suv39h1 status, probably because constitutive Myc expression firmly represses these promoters *via* Miz-1 (Seoane et al., 2002; Spender and Inman, 2009) (Figure S3E, and transcriptional levels by RQ-PCR, data not shown). Unlike γ-irradiation, TGF-β1 treatment of lymphoid cells failed to produce DNA lesions (Figure S3F and S3G), and was not accompanied by elevated ROS levels either (data not shown). Of note, H_2O_2-induced DNA damage, at levels comparable to DNA damage evoked by oncogenic Myc, synergized with TGF-β to promote cellular senescence (Figure S3G, compare to γ-H2AX foci in Figure S2A), as seen for Myc induction and TGF-β treatment in MEFs (Figure S3H). Accordingly, DDR-defective *ATM*$^{-/-}$ lymphomas senesced in response to TGF-β1 as control (or, likewise, $p16^{INK4a}$- or $p21^{CIP1}$-deficient) lymphomas did, while p53-null lymphomas were expectedly refractory (Cordenonsi et al., 2003) (Figure 3D). Hence, TGF-β promotes cellular senescence without damaging DNA, but cooperatively with oncogene-related DDR signaling in a Myc-primed and p53/Suv39h1-dependent fashion.

Next, we aimed to identify the cellular source of the considerable amounts of TGF-β detectable in Eμ-*myc* lymphoma tissues. Importantly, lymphoma cells did not secrete TGF-β1 above culture medium background levels (Figure S3I). However, freshly isolated lymphoma cells exhibited Smad3 phosphorylation (Smad3-P), a mark of activated TGF-β signaling, while Smad3-P was undetectable in freshly isolated pre-neoplastic Eμ-*myc* transgenic B-cells (Figure S3J; see also Figure S1C). Likewise, no Smad3-P signal was found in non-transgenic B-cells following transduction with a Myc expression construct, indicating that Myc *per se* is incapable of driving TGF-β expression. Notably, the recently observed link between oncogene-induced senescence and a senescence-reinforcing pro-inflammatory secretory phenotype, termed 'SASP' (Acosta et al., 2008; Coppe et al., 2008; Kuilman et al., 2008; Wajapeyee et al., 2008), raised the questions whether TGF-β1 might be a component or a regulator of the SASP-related cytokines. However, RQ-PCR analysis of a panel of SASP candidates in Myc-

lymphomas of various genotypes exposed to senescence-inducing H_2O_2 or TGF-β1 unveiled substantial SASP induction only in senescence-capable control lymphomas following exposure to H_2O_2 but not to TGF-β1. Moreover, TGF-β1 itself does not belong to the SASP signature of lymphoma cells, which is different from fibroblasts that expressed increased amounts of TGF-β1 upon γ-irradiation or H_2O_2 (Figure S3K-M). In essence, neither proliferating nor senescent lymphoma cells secrete significant amounts of TGF-β, implying that TGF-β might be provided by non-neoplastic bystander cells.

Apoptotic Lymphoma Cells Activate Macrophages to Secrete Pro-Senescent TGF-β1

We considered lymphoma-infiltrating and -activated macrophages to serve as a non-cell-autonomous source of TGF-β1 *in vivo*, since macrophages reportedly secrete TGF-β1 upon phosphatidylserine (PS)-dependent ingestion of apoptotic cells (Huynh et al., 2002; Savill and Fadok, 2000), which are typically found at significant frequencies in Myc-driven lymphomas (Figure 1B, and Figure S4A for the phenotypic characterization of lymphoma-infiltrating macrophages). Indeed, co-culture of macrophages with PS-positive apoptotic, but not with PS-negative proliferating lymphoma cells resulted in increased TGF-β1 secretion, as alternatively observed upon stimulation of macrophages with PMA (phorbol 12-myristate 13-acetate; Figure 4A and Figure S4B). Consistently, lymphomas harboring a robust Bcl2-mediated apoptotic block (control/bcl2; see also ref. (Schmitt et al., 2002b)) presented with a much lower frequency of both infiltrating macrophages and senescent cells *in vivo* (Figure 4B and Figure S4C, see also Figure 1G and Figure S1D for a correlation between senescent cells and infiltrating macrophages in various lymphoma genotypes). The nearly

complete absence of senescent control;bcl2 lymphoma cells *in vivo* despite their *in vitro*-susceptibility to TGF-β-mediated senescence (Figure 3B) underscores the importance of non-cell-autonomous events such as attraction of macrophages (Lauber et al., 2003) and their subsequent activation by apoptotic lymphoma cells to secrete TGF-β1.

To further elucidate the pro-senescent role of activated macrophages *in vivo*, we adoptively transferred PMA-stimulated Ana-1 macrophages into mice harboring Myc-driven lymphomas. GFP-tagged Ana-1 cells homed to lymphoma sites, and their presence correlated with enhanced TGF-β1 pathway activation (*i.e.* Smad3-P), induction of the TGF-β target and senescence indicator plasminogen activator inhibitor-1 (PAI-1), and, most notably, with a substantial increment of senescent lymphoma cells (Figure 4C, and Figure S4D and S4E). Conversely, systemic depletion of macrophages by repetitive provision of liposome-encapsulated clodronate (Aichele et al., 2003) significantly lowered the number of lymphoma-infiltrating macrophages, Smad3 activation (*i.e.* Smad3-P), and, most importantly, lymphoma cell senescence (Figure 4D, and Figure S4F and S4G; for effects of pharmacological inhibition of TGF-β production see Figure S4H-J).

To confirm the impact of TGF-β on senescence induction *in vivo*, we sought to locally block its action by expressing a soluble, secretable TGF-β1-neutralizing TGF-β type II receptor extracellular domain (TβR-II-ED), thereby restricting TGF-β inhibition to the vicinity of TβR-II-ED-expressing cells (Thomas and Massague, 2005). Importantly, transplantation of Eμ-*myc* transgenic hematopoietic stem cells stably transduced with TβR-II-ED into lethally irradiated recipient mice resulted in a profoundly accelerated onset of lymphomas ($P < 0.0001$); these lymphomas virtually lacked Smad3 phosphorylation and displayed, despite unaffected macrophage frequencies, much less senescent cells when compared to a mock-infected cohort

(Figure 4E and 4F and Figure S4K-M). Tumor latency remained unchanged when the TβR-II-ED moiety was tested in Suv39h1-deficient hematopoietic stem cells, indicating that TGF-β-mediated apoptosis has no significant tumor-delaying impact in this model (data not shown). Furthermore, when matched pairs of primary lymphomas were propagated in immunocompetent recipients, TβR-II-ED-expressing lymphomas always formed with lower senescence frequencies than the corresponding empty vector samples (Figure 4G). Thus, selective ablation of TGF-β action reduces lymphoma cell senescence in tumor development and in otherwise genetically identical lymphoma aliquots during tumor expansion *in vivo*. Importantly, these results, like the sharply reduced senescence frequency in Bcl2-protected lymphomas *in vivo* (Figure 4B), clarify that the non-cell-autonomous induction of senescence is quantitatively substantially more relevant than the cell-autonomous signaling cascade into senescence (as addressed in Figure 2).

Ultimately, we aimed to dissect the sequential process of lymphoma cell apoptosis-induced macrophage-derived TGF-β action on lymphoma cell senescence in a single *in vitro* experiment. To this end, we co-incubated Bcl2-protected lymphoma cells with macrophages, which were activated by exposure to apoptotic lymphoma cells beforehand, with or without a pharmacological TGF-β receptor type I inhibitor (TGFR-I). Indeed, only apoptotic body-activated macrophages produced a more than 3-fold increase of SA-β-gal-positive lymphoma cells that was largely abolished in the presence of the TGFR-I (Figure 4H and Figure S4N). Therefore, TGF-β secreted by macrophages upon their activation by apoptotic lymphoma cells indeed acts as a critical stroma-derived inducer of lymphoma cell senescence.

To test whether the proposed, mouse model-deduced mechanism of non-cell-autonomous senescence induction may apply to human aggressive B-cell lymphomas as well, we analyzed its central components in a panel of 30 diffuse large B-cell lymphoma

samples. The panel was sub-divided based on Ki67 immunoreactivity into a very high proliferation ($Ki67^{hi}$; ≥ 80% Ki67-positive cells) and a lower proliferation ($Ki67^{lo}$; < 80% Ki67-positive cells) group. Indeed, $Ki67^{lo}$ samples exhibited a significantly higher frequency of H3K9me3-positive cells, indicative of cellular senescence in paraffin-embedded sections that cannot be examined for enzymatic SA-β-gal activity (Figure 5A and 5B). Importantly, the $Ki67^{lo}$ group also presented with a higher fraction of apoptotic cells, more lymphoma-infiltrating macrophages, and a stronger reactivity for the TGF-β signaling mediator Smad3-P (Figure 5B). Thus, these data strongly suggest that environmentally co-controlled tumor cell senescence plays an important growth-restraining role in human aggressive B-cell lymphomas as well.

DISCUSSION

Our data establish a model of senescence induction in an oncogenic context where the primary cellular response to the driving oncogene is overt apoptosis, not senescence. Elegant work elucidating signaling cascades involved in RAS-, BRAF-, or MEK-type oncogene-induced senescence demonstrated that an oncogene-evoked DDR (Bartkova et al., 2006; Di Micco et al., 2006; Mallette et al., 2007), a global negative feedback response attenuating RAS effector signaling (Courtois-Cox et al., 2006), and, most recently, pro-inflammatory cytokines acting as reinforcing networks (Acosta et al., 2008; Coppe et al., 2008; Kuilman et al., 2008; Wajapeyee et al., 2008) contribute to the senescence phenotype. However, all of these studies view senescence as a cell-autonomous phenomenon in which, if at all, cellular interactions or secreted factors promote the senescent arrest in a homotypic self-amplifying way. We report here an oncogene-initiated but non-cell-autonomous route into senescence. This process depends on the activation of TGF-β1-secreting non-neoplastic cells as a critical

intermediate step, linking Myc-provoked cell-autonomous apoptosis to the subsequent senescence induction of a significant proportion of the remaining tumor cells by the stromal cytokine (Figure 5C). Hence, our data demonstrate that apoptosis and senescence are not simply two context-dependent choices of cellular stress responsiveness, but that they can be enforced in an interdependent fashion on the organismic level. In this regard, disrupted DNA damage signaling may not only compromise cell-autonomous induction of cellular senescence (Figure 1G, Figure 2D and Figure S2E and S2F), but might also anticipate impaired macrophage-related senescence due to reduced primary apoptosis. Importantly, DDR-defective tumor cells remain susceptible to non-DNA damaging pro-senescent stimuli that might be therapeutically exploited in the future. Moreover, our data underscore why p53 inactivation – blocking apoptosis, preventing macrophage attraction, and rendering the cell insensitive to TGF-β-induced senescence – is a particularly efficient way to escape Myc-related senescence.

We would like to emphasize that 12-20% senescent cells, which were detectable in control lymphomas at diagnosis, are indeed likely to account for a substantial delay in tumor formation. These frequencies reflect “snap-shots” of a dynamic process that involves rapid clearance of senescent cells by the host immune system (J.R.D. and C.A.S., manuscript in preparation), as recently reported for a mouse model presenting with senescent liver cancer cells (Xue et al., 2007). The profound impact on overall tumor growth of relatively small steady-state proportions of cells that exited the cycle is well established in the apoptosis field and seems to apply to senescent cells in a comparable way.

Of note, cellular and secreted components that delay tumor manifestation *via* senescence as shown here do not necessarily keep operating as tumor constraints during later steps of cancer progression, as there is ample evidence that both tumor-associated

macrophages and TGF-β can produce deleterious effects by promoting tumor growth or by exerting tolerogenic immune effects (Dave et al., 2004; Thomas and Massague, 2005). However, TGF-β1 signaling has just been reported as a component of the prognostically favorable "stromal-1" signature in human diffuse large B-cell lymphoma (Lenz et al., 2008), a frequently Myc-activated entity in which we identified here a subgroup with features highly reminiscent of the presented mechanism of macrophage-mediated senescence induction that we genetically dissected in the murine Eμ-*myc* model of aggressive B-cell lymphoma.

Furthermore, our findings characterize the Rb-related Suv39h1-mediated H3K9me3/HP1 heterochromatin mark as a rather universal and essential downstream effector module of the senescence program that is still operational in the presence of constitutive Myc signaling. This chromatin mark is produced not only by activated oncogenes or DNA damaging chemotherapy (Braig et al., 2005; Collado et al., 2005; Michaloglou et al., 2005) but also by the cytostatic action of secretory TGF-β. Given the anti-cancer relevance of cellular senescence, the now demonstrated inducibility of senescence by a non-DNA damaging cytokine opens the exciting perspective to utilize Suv39h1/H3K9me3-enforcing approaches for future cancer therapies.

EXPERIMENTAL PROCEDURES

Lymphoma Analysis and *In vivo*-Treatments

All animal protocols used in this study were approved by the governmental review board (Landesamt Berlin), and conform to the respective regulatory standards. Lymphomas with defined genetic defects were generated by intercrossing Eμ-*myc* transgenic mice with mice carrying loss-of-function alleles at the *Suv39h1*, the *p53*, the

INK4a/ARF, the *CIP1* or the *ATM* locus, all in a C57BL/6 background (Adams et al., 1985; Barlow et al., 1996; Christophorou et al., 2005; Deng et al., 1995; Jacks et al., 1994; Kamijo et al., 1997; Krimpenfort et al., 2001; Peters et al., 2001). Genotyping of the offspring by allele-specific genomic PCR, monitoring of lymphoma onset, preservation of snap-frozen or formalin-fixed lymph node tissue and isolation of viable lymphoma cells, splenic B-lymphocytes (*via* magnetic bead selection [B-cell isolation kit, Miltenyi]), fetal liver cells (FLC), primary peritoneal macrophages (pMP) or mouse embryo fibroblasts (MEF) were carried out as described (Davies and Gordon, 2005; Reimann et al., 2007; Schmitt et al., 2002a; Schmitt et al., 2002b). Where indicated, B-cells were pre-stimulated for 48 hours with 5 µg lipopolysaccharide (LPS)/ml (from Salmonella enterica; Sigma-Aldrich). Pre-neoplastic cells were obtained from approximately 30-days-old Eµ-*myc* transgenic animals devoid of lymph node or spleen enlargement and with no evidence of leukemia by blood smear analysis. In some experiments, mice were exposed to specific drug treatments as described in the Supplemental Experimental Procedures. The use of tumor biopsies primarily obtained for the initial diagnosis of diffuse large B-cell lymphoma as anonymous samples was approved by the local ethics commission of Charité - Universitätsmedizin Berlin (reference EA4/085/07). Detection of apoptotic DNA strand breaks by TUNEL (terminal deoxynucleotidyl transferase dUTP nick end labeling; Roche) staining in paraffin-embedded tissue sections and assessment of SA-β-gal activity at pH 5.5 in cryosections or cytospin preparations of cell suspensions were carried out as described (Schmitt et al., 2002a; Schmitt et al., 1999). Eµ-*myc* transgenic FLC as a source of hematopoietic stem cells were obtained to reconstitute (sub-)lethally (*i.e.* a single 6 or 10 Gy-dose of total body γ-irradiation) irradiated non-transgenic recipient mice. FLC, splenic B-lymphocytes, isolated lymphoma cells (typically on irradiated NIH3T3 fibroblasts serving as feeders), macrophages and MEFs were cultured in liquid medium or semi-solid methylcellulose as described (Schmitt et al., 1999; Schmitt et al., 2000),

and stably transduced with MSCV-c-Myc-IRES-GFP, MSCV-HA-Suv39h1-puro (kindly provided as pcDNA3.1-HA-Suv39h1 by A. Leutz), MSCV-bcl2-blasticidine, MSCV-bcl2-puro, pBabe-c-MycER^{TAM}-puro (a generous gift from M. Eilers) or the GFP co-encoding retroviruses MSCV-IRES-GFP and MSCV-TβR-II-ED-IRES-GFP (kindly provided as MSCV-TβR-II-ED-puro by J. Massagué) (Reimann et al., 2007; Schmitt et al., 1999; Schmitt et al., 2002b); the C57BL/6-derived Ana-1 macrophages (kindly provided by L. Varesio) were GFP-transduced *via* nucleofection (nucleofector kit V, Lonza). In some settings, macrophages were treated *in vitro* with phorbol 12-myristate 13-acetate (PMA; Sigma), lisinopril, or adriamycin (Sigma) for the indicated times and at the indicated concentrations.

Analysis of Growth Parameters, Chromosomal Abnormalities and DNA Damage

In some experiments, lymphoma cells were exposed *in vitro* to purified human TGF-β1 (R&D Systems) at 100 or 1000 pM, or were treated with 1 μM 4-hydroxy-tamoxifen (4-OHT; Sigma-Aldrich) or the equivalent volume of the ethanol-based solvent, or were incubated with H_2O_2 (100 μM; Sigma-Aldrich), or were exposed to the TGF-β R I inhibitor V (SD-208; 500 nM; Calbiochem/Merck) for the indicated times, or were treated with NAC or caffeine (Sigma-Aldrich) as stated. Viability and cell numbers were analyzed by trypan blue dye exclusion, cell-cycle parameters by BrdU and propidium iodide (PI) staining (Schmitt et al., 1999; Schmitt et al., 2002b). For numeric karyotypic analysis, at least twelve DAPI stained metaphases were counted per lymphoma sample (Schmitt et al., 2002b). Cytospin preparations of suspension cultures for subsequent SA-β-gal analyses or immunostainings, quantification of ROS by 2'-7'-dichlordihydrofluorescein-based flow cytometric analyses, and quantification of DNA strand breaks in Annexin V-negative cells (Miltenyi) by the Comet assay were carried out as previously described (Braig et al., 2005; Reimann et al., 2007).

Gene Expression Analysis

Genome-wide expression analysis was performed on RNA isolated with Trizol (Invitrogen) from whole lymph nodes derived from individual lymphoma-bearing mice and from normal spleen as control, or, in a second set of experiments, from short-term cultured lymphoma cells with and without exposure to 100 pM of human TGF-β1 for 24 hours using a 22.5 K mouse cDNA array. For RT-PCR analyses, RNA extracts were transcribed into cDNA using SuperScript reverse transcriptase (Invitrogen) and random hexamers or oligo-dT. Primer sequences and detailed PCR protocols for the detection of murine *ACE*, *Suv39h1*, *Suv39h2*, *TβRII-ED*, and *TATA box binding protein* (*TBP*; as an internal control) transcripts as well as for the RQ-PCR analyses of mouse *CIP1*, *CTGF*, *CXCL1*, *CXCL7*, *CXCL16*, *GAPDH*, *GM-CSF*, *IGFBP6*, *IGFBP7*, *IL-1α*, *IL-6*, *IL-7*, *INK4b*, *MCP-4*, *MIP-3α*, *MMP2*, *MMP3*, *Tgfig*, *TGF-β1*, *TGF-β2*, *TGF-β3*, and *VEGF* transcripts (using commercially available primers; Applied Biosystems) are available upon request. For every given sample, ΔCt values were determined as the difference between the Ct value of a specific transcript and the Ct value of *GAPDH*, serving as the housekeeping control mRNA, and relative transcript levels (*e.g.* treated *vs.* untreated) were then produced based on $2^{(-\Delta\Delta Ct)}$ with $\Delta\Delta Ct = \Delta Ct_{treated} - \Delta Ct_{untreated}$.

Immunophenotyping by flow cytometry as well as antigen detection by immunofluorescence (IF), immunohistochemistry (IHC), immunoblotting (IB), and immunoprecipitation (IP) was carried out as described (Reimann et al., 2007; Schmitt et al., 2002a). A summary of the methods and the complete list of antibodies used can be found in the Supplemental Experimental Procedures. Staining intensities of Smad3-P or PAI-1 *in situ* were semi-quantitatively assessed (- *vs.* +, ++ or +++; converted into numeric values 0, 1, 2 or 3 to calculate a mean in some experiments [where a value of

around 0.5 would translate into (+)]). TGF-β1 protein concentrations were also measured by ELISA (Quantikine, R&D Systems) in HCl-activated cell-free culture supernatant in accordance with the manufacturer's protocol.

Statistical Evaluation

Tumor onset data reflecting the latency between birth and first-time palpability of enlarged lymph nodes were compared using the log-rank (Mantel-Cox) test. Curve fitting analysis was done by linear regression with R^2 as the coefficient of determination. The unpaired t-test was used to compare means and standard deviations (SD). All quantifications from staining reactions (*e.g.* immunostainings, TUNEL or SA-β-gal assays) were carried out by an independent and blinded second examiner, and reflect at least three samples with at least 200 events counted (typically in more than three different tissue areas) each.

Accession Numbers

Details about the cDNA microarray protocols, the specific array design, and the respective data can be found at http://www.ebi.ac.uk/arrayexpress/ under accession number E-MEXP-1423 for the first set and E-MEXP-1424 for the second set of experiments.

SUPPLEMENTAL DATA

Supplemental data include Supplemental Experimental Procedures, Supplemental References, and four figures, and can be found with this article online at http://www.cell.com/cancer-cell/supplemental/xxx.

ACKNOWLEDGMENTS

We thank C. Barlow, M. Eilers, G. Evan, the late A. Harris, T. Jacks, P. Krimpenfort, P. Leder and J. Sherr for mice, B. Falini, A. Leutz, J. Massagué and L. Varesio for mice, cells, and materials, A. Lude, S. Maßwig, N. Mikuda, I. Nehlmeier, M. Schmock and S. Spieckermann for technical assistance, and members of the Schmitt lab for discussions and editorial advice. This work was supported by a Ph.D. fellowship to J.R.D. from the Boehringer Ingelheim Foundation, and grants to C.A.S. from the European Union, the Deutsche Forschungsgemeinschaft (KFO105 and TRR54) and the Deutsche Krebshilfe.

REFERENCES

Acosta, J. C., O'Loghlen, A., Banito, A., Guijarro, M. V., Augert, A., Raguz, S., Fumagalli, M., Da Costa, M., Brown, C., Popov, N.*, et al.* (2008). Chemokine signaling via the CXCR2 receptor reinforces senescence. Cell *133*, 1006-1018.

Adams, J. M., Harris, A. W., Pinkert, C. A., Corcoran, L. M., Alexander, W. S., Cory, S., Palmiter, R. D., and Brinster, R. L. (1985). The c-myc oncogene driven by immunoglobulin enhancers induces lymphoid malignancy in transgenic mice. Nature *318*, 533-538.

Aichele, P., Zinke, J., Grode, L., Schwendener, R. A., Kaufmann, S. H., and Seiler, P. (2003). Macrophages of the splenic marginal zone are essential for trapping of blood-borne particulate antigen but dispensable for induction of specific T cell responses. J Immunol *171*, 1148-1155.

Barlow, C., Hirotsune, S., Paylor, R., Liyanage, M., Eckhaus, M., Collins, F., Shiloh, Y., Crawley, J. N., Ried, T., Tagle, D., and Wynshaw-Boris, A. (1996). Atm-deficient mice: a paradigm of ataxia telangiectasia. Cell *86*, 159-171.

Bartkova, J., Rezaei, N., Liontos, M., Karakaidos, P., Kletsas, D., Issaeva, N., Vassiliou, L. V., Kolettas, E., Niforou, K., Zoumpourlis, V. C.*, et al.* (2006). Oncogene-induced senescence is part of the tumorigenesis barrier imposed by DNA damage checkpoints. Nature *444*, 633-637.

Braig, M., Lee, S., Loddenkemper, C., Rudolph, C., Peters, A. H., Schlegelberger, B., Stein, H., Dorken, B., Jenuwein, T., and Schmitt, C. A. (2005). Oncogene-induced senescence as an initial barrier in lymphoma development. Nature *436*, 660-665.

Campisi, J., and d'Adda di Fagagna, F. (2007). Cellular senescence: when bad things happen to good cells. Nat Rev Mol Cell Biol *8*, 729-740.

Christophorou, M. A., Martin-Zanca, D., Soucek, L., Lawlor, E. R., Brown-Swigart, L., Verschuren, E. W., and Evan, G. I. (2005). Temporal dissection of p53 function in vitro and in vivo. Nat Genet *37*, 718-726.

Collado, M., Gil, J., Efeyan, A., Guerra, C., Schuhmacher, A. J., Barradas, M., Benguria, A., Zaballos, A., Flores, J. M., Barbacid, M.*, et al.* (2005). Tumour biology: senescence in premalignant tumours. Nature *436*, 642.

Coppe, J. P., Patil, C. K., Rodier, F., Sun, Y., Munoz, D. P., Goldstein, J., Nelson, P. S., Desprez, P. Y., and Campisi, J. (2008). Senescence-associated secretory phenotypes reveal cell-nonautonomous functions of oncogenic RAS and the p53 tumor suppressor. PLoS Biol *6*, 2853-2868.

Cordenonsi, M., Dupont, S., Maretto, S., Insinga, A., Imbriano, C., and Piccolo, S. (2003). Links between tumor suppressors: p53 is required for TGF-beta gene responses by cooperating with Smads. Cell *113*, 301-314.

Courtois-Cox, S., Genther Williams, S. M., Reczek, E. E., Johnson, B. W., McGillicuddy, L. T., Johannessen, C. M., Hollstein, P. E., MacCollin, M., and Cichowski, K. (2006). A negative feedback signaling network underlies oncogene-induced senescence. Cancer Cell *10*, 459-472.

Dave, S. S., Wright, G., Tan, B., Rosenwald, A., Gascoyne, R. D., Chan, W. C., Fisher, R. I., Braziel, R. M., Rimsza, L. M., Grogan, T. M., *et al.* (2004). Prediction of survival in follicular lymphoma based on molecular features of tumor-infiltrating immune cells. N Engl J Med *351*, 2159-2169.

Davies, J. Q., and Gordon, S. (2005). Isolation and culture of human macrophages. Methods Mol Biol *290*, 105-116.

Deng, C., Zhang, P., Harper, J. W., Elledge, S. J., and Leder, P. (1995). Mice lacking p21CIP1/WAF1 undergo normal development, but are defective in G1 checkpoint control. Cell *82*, 675-684.

Di Micco, R., Fumagalli, M., Cicalese, A., Piccinin, S., Gasparini, P., Luise, C., Schurra, C., Garre, M., Nuciforo, P. G., Bensimon, A., *et al.* (2006). Oncogene-induced senescence is a DNA damage response triggered by DNA hyper-replication. Nature *444*, 638-642.

Dimri, G. P., Lee, X., Basile, G., Acosta, M., Scott, G., Roskelley, C., Medrano, E. E., Linskens, M., Rubelj, I., Pereira-Smith, O., and et al. (1995). A biomarker that identifies senescent human cells in culture and in aging skin in vivo. Proc Natl Acad Sci U S A *92*, 9363-9367.

Dokmanovic, M., Chang, B. D., Fang, J., and Roninson, I. B. (2002). Retinoid-induced growth arrest of breast carcinoma cells involves co-activation of multiple growth-inhibitory genes. Cancer Biol Ther *1*, 24-27.

Egle, A., Harris, A. W., Bouillet, P., and Cory, S. (2004). Bim is a suppressor of Myc-induced mouse B cell leukemia. Proc Natl Acad Sci U S A *101*, 6164-6169.

Evan, G. I., Wyllie, A. H., Gilbert, C. S., Littlewood, T. D., Land, H., Brooks, M., Waters, C. M., Penn, L. Z., and Hancock, D. C. (1992). Induction of apoptosis in fibroblasts by c-myc protein. Cell *69*, 119-128.

Feldser, D. M., and Greider, C. W. (2007). Short telomeres limit tumor progression in vivo by inducing senescence. Cancer Cell *11*, 461-469.

Grandori, C., Wu, K. J., Fernandez, P., Ngouenet, C., Grim, J., Clurman, B. E., Moser, M. J., Oshima, J., Russell, D. W., Swisshelm, K., *et al.* (2003). Werner syndrome protein limits MYC-induced cellular senescence. Genes Dev *17*, 1569-1574.

Guney, I., Wu, S., and Sedivy, J. M. (2006). Reduced c-Myc signaling triggers telomere-independent senescence by regulating Bmi-1 and p16(INK4a). Proc Natl Acad Sci U S A *103*, 3645-3650.

Hans, C. P., Weisenburger, D. D., Greiner, T. C., Gascoyne, R. D., Delabie, J., Ott, G., Muller-Hermelink, H. K., Campo, E., Braziel, R. M., Jaffe, E. S., *et al.* (2004). Confirmation of the molecular classification of diffuse large B-cell lymphoma by immunohistochemistry using a tissue microarray. Blood *103*, 275-282.

Hemann, M. T., and Narita, M. (2007). Oncogenes and senescence: breaking down in the fast lane. Genes Dev *21*, 1-5.

Huynh, M. L., Fadok, V. A., and Henson, P. M. (2002). Phosphatidylserine-dependent ingestion of apoptotic cells promotes TGF-beta1 secretion and the resolution of inflammation. J Clin Invest *109*, 41-50.

Jacks, T., Remington, L., Williams, B. O., Schmitt, E. M., Halachmi, S., Bronson, R. T., and Weinberg, R. A. (1994). Tumor spectrum analysis in p53-mutant mice. Curr Biol *4*, 1-7.

Kamijo, T., Zindy, F., Roussel, M. F., Quelle, D. E., Downing, J. R., Ashmun, R. A., Grosveld, G., and Sherr, C. J. (1997). Tumor suppression at the mouse INK4a locus mediated by the alternative reading frame product p19ARF. Cell *91*, 649-659.

Kramata, P., Lu, Y. P., Lou, Y. R., Cohen, J. L., Olcha, M., Liu, S., and Conney, A. H. (2005). Effect of administration of caffeine or green tea on the mutation profile in the p53 gene in early mutant p53-positive patches of epidermal cells induced by chronic UVB-irradiation of hairless SKH-1 mice. Carcinogenesis *26*, 1965-1974.

Krimpenfort, P., Quon, K. C., Mooi, W. J., Loonstra, A., and Berns, A. (2001). Loss of p16Ink4a confers susceptibility to metastatic melanoma in mice. Nature *413*, 83-86.

Kuilman, T., Michaloglou, C., Vredeveld, L. C., Douma, S., van Doorn, R., Desmet, C. J., Aarden, L. A., Mooi, W. J., and Peeper, D. S. (2008). Oncogene-induced senescence relayed by an interleukin-dependent inflammatory network. Cell *133*, 1019-1031.

Lachner, M., O'Carroll, D., Rea, S., Mechtler, K., and Jenuwein, T. (2001). Methylation of histone H3 lysine 9 creates a binding site for HP1 proteins. Nature *410*, 116-120.

Laiho, M., DeCaprio, J. A., Ludlow, J. W., Livingston, D. M., and Massague, J. (1990). Growth inhibition by TGF-beta linked to suppression of retinoblastoma protein phosphorylation. Cell *62*, 175-185.

Lauber, K., Bohn, E., Krober, S. M., Xiao, Y. J., Blumenthal, S. G., Lindemann, R. K., Marini, P., Wiedig, C., Zobywalski, A., Baksh, S.*, et al.* (2003). Apoptotic cells induce migration of phagocytes via caspase-3-mediated release of a lipid attraction signal. Cell *113*, 717-730.

Lee, A. C., Fenster, B. E., Ito, H., Takeda, K., Bae, N. S., Hirai, T., Yu, Z. X., Ferrans, V. J., Howard, B. H., and Finkel, T. (1999). Ras proteins induce senescence by altering the intracellular levels of reactive oxygen species. J Biol Chem *274*, 7936-7940.

Lenz, G., Wright, G., Dave, S. S., Xiao, W., Powell, J., Zhao, H., Xu, W., Tan, B., Goldschmidt, N., Iqbal, J.*, et al.* (2008). Stromal Gene Signatures in Large-B-Cell Lymphomas. N Engl J Med *359*, 2313-2323.

Lin, H. K., Bergmann, S., and Pandolfi, P. P. (2004). Cytoplasmic PML function in TGF-beta signalling. Nature *431*, 205-211.

Mallette, F. A., Gaumont-Leclerc, M. F., and Ferbeyre, G. (2007). The DNA damage signaling pathway is a critical mediator of oncogene-induced senescence. Genes Dev *21*, 43-48.

Martins, C. P., Brown-Swigart, L., and Evan, G. I. (2006). Modeling the therapeutic efficacy of p53 restoration in tumors. Cell *127*, 1323-1334.

Michaloglou, C., Vredeveld, L. C., Soengas, M. S., Denoyelle, C., Kuilman, T., van der Horst, C. M., Majoor, D. M., Shay, J. W., Mooi, W. J., and Peeper, D. S. (2005). BRAFE600-associated senescence-like cell cycle arrest of human naevi. Nature *436*, 720-724.

Narita, M., Nunez, S., Heard, E., Lin, A. W., Hearn, S. A., Spector, D. L., Hannon, G. J., and Lowe, S. W. (2003). Rb-mediated heterochromatin formation and silencing of E2F target genes during cellular senescence. Cell *113*, 703-716.

Peters, A. H., O'Carroll, D., Scherthan, H., Mechtler, K., Sauer, S., Schofer, C., Weipoltshammer, K., Pagani, M., Lachner, M., Kohlmaier, A*., et al.* (2001). Loss of the Suv39h histone methyltransferases impairs mammalian heterochromatin and genome stability. Cell *107*, 323-337.

Reimann, M., Loddenkemper, C., Rudolph, C., Schildhauer, I., Teichmann, B., Stein, H., Schlegelberger, B., Dorken, B., and Schmitt, C. A. (2007). The Myc-evoked DNA damage response accounts for treatment resistance in primary lymphomas in vivo. Blood *110*, 2996-3004.

Savill, J., and Fadok, V. (2000). Corpse clearance defines the meaning of cell death. Nature *407*, 784-788.

Schmitt, C. A., Fridman, J. S., Yang, M., Lee, S., Baranov, E., Hoffman, R. M., and Lowe, S. W. (2002a). A senescence program controlled by p53 and p16INK4a contributes to the outcome of cancer therapy. Cell *109*, 335-346.

Schmitt, C. A., McCurrach, M. E., de Stanchina, E., Wallace-Brodeur, R. R., and Lowe, S. W. (1999). INK4a/ARF mutations accelerate lymphomagenesis and promote chemoresistance by disabling p53. Genes Dev *13*, 2670-2677.

Schmitt, C. A., Rosenthal, C. T., and Lowe, S. W. (2000). Genetic analysis of chemoresistance in primary murine lymphomas. Nat Med *6*, 1029-1035.

Schmitt, C. A., Yang, M., Fridman, J. S., Baranov, E., Hoffman, R. M., and Lowe, S. W. (2002b). Dissecting p53 tumor suppressor functions in vivo. Cancer Cell *1*, 289-298.

Schwarz, J. K., Bassing, C. H., Kovesdi, I., Datto, M. B., Blazing, M., George, S., Wang, X. F., and Nevins, J. R. (1995). Expression of the E2F1 transcription factor overcomes type beta transforming growth factor-mediated growth suppression. Proc Natl Acad Sci U S A *92*, 483-487.

Seoane, J., Le, H. V., and Massague, J. (2002). Myc suppression of the p21(Cip1) Cdk inhibitor influences the outcome of the p53 response to DNA damage. Nature *419*, 729-734.

Serrano, M., Lin, A. W., McCurrach, M. E., Beach, D., and Lowe, S. W. (1997). Oncogenic ras provokes premature cell senescence associated with accumulation of p53 and p16INK4a. Cell *88*, 593-602.

Spender, L. C., and Inman, G. J. (2009). TGF-beta induces growth arrest in Burkitt lymphoma cells via transcriptional repression of E2F-1. J Biol Chem *284*, 1435-1442.

Strasser, A., Harris, A. W., Bath, M. L., and Cory, S. (1990). Novel primitive lymphoid tumours induced in transgenic mice by cooperation between myc and bcl-2. Nature *348*, 331-333.

Thomas, D. A., and Massague, J. (2005). TGF-beta directly targets cytotoxic T cell functions during tumor evasion of immune surveillance. Cancer Cell *8*, 369-380.

Vafa, O., Wade, M., Kern, S., Beeche, M., Pandita, T. K., Hampton, G. M., and Wahl, G. M. (2002). c-Myc can induce DNA damage, increase reactive oxygen species, and mitigate p53 function: a mechanism for oncogene-induced genetic instability. Mol Cell *9*, 1031-1044.

Wajapeyee, N., Serra, R. W., Zhu, X., Mahalingam, M., and Green, M. R. (2008). Oncogenic BRAF induces senescence and apoptosis through pathways mediated by the secreted protein IGFBP7. Cell *132*, 363-374.

Xue, W., Zender, L., Miething, C., Dickins, R. A., Hernando, E., Krizhanovsky, V., Cordon-Cardo, C., and Lowe, S. W. (2007). Senescence and tumour clearance is triggered by p53 restoration in murine liver carcinomas. Nature *445*, 656-660.

FIGURE LEGENDS

Figure 1. Suv39h1-Dependent Senescence Attenuates Myc-Driven Lymphomagenesis

(A) Latencies to palpable lymphoma manifestation in Eμ-*myc* transgenic mice (control lymphoma, $n = 93$, black), in Eμ-*myc*;*Suv39h1*$^{+/-}$ ($n = 41$, red), and in Eμ-*myc*;*Suv39h1*$^{-}$ mice ($n = 31$, orange). Insert: *Suv39h1* mRNA expression by RT-PCR analysis of short-term cultured lymphomas derived from *Suv39h1*$^{+/-}$ mice ($n = 4$) with a *Suv39h1*$^{+/+}$ derived lymphoma for comparison; *TBP* as an internal control.

(B) Growth-related parameters, *i.e.* apoptosis by TUNEL reactivity, and senescence by SA-β-gal staining in lymph node sections obtained at manifestation from Eμ-*myc* control or *Suv39h1*$^{-}$ lymphomas (representative photomicrographs from at least nine samples per genotype tested).

(C) Percentages of SA-β-gal-positive cells (as in b) in individual control ($n = 25$) and *Suv39h1*$^{-}$ ($n = 9$) lymphomas. Horizontal lines represent the mean percentage of each group. Note that low-level SA-β-gal-positive cases in the control group are enriched for spontaneously *p53* mutant or homozygously *INK4a/ARF*-deleted lymphomas (Schmitt et al., 1999) (data not shown).

(D) Percentages of Ki67-positive (red) and BrdU-positive cells (brown; note the mutually exclusive SA-β-gal-co-staining [blue]) *in situ*, and quantification of H3K9me3^{high}/Ki67^{low} cells (arrow-marked gate, representing senescent cells) by flow cytometry in control and *Suv39h1*$^{-}$ lymphomas.

(E) Immunoblot analyses of the indicated proteins in individual control (lanes 1-4) and *Suv39h1*$^{-}$ (lanes 5-8) lymphoma cell lysates with α-Tubulin as a loading control (arrow indicates the hypophosphorylated [hypo-P] Rb band representing cells in G1).

(F) Genomic status of the *p53* locus by allele-specific PCR (top) and expression status of *Suv39h1* transcripts by RT-PCR (bottom; *TBP* as an internal control) analyses of short-term cultured lymphoma cells that were isolated from mice of the indicated genotypes. Extracts from *p53*$^{+/-}$ and *p53*$^{-/-}$ MEFs as controls.

(G) Frequencies of SA-β-gal-positive cells in Eμ-*myc* lymphoma cryosections of the indicated genotypes at diagnosis (control and *Suv39h1*$^{-}$ as in b, at least four cases per genotype tested).

All numbers indicate the mean percentages of positive cells ± SD; "*" reflects $P < 0.05$. All scale bars = 50 μm (identical magnification throughout the panel). See also Figure S1.

Figure 2. Myc has p53-Dependent Pro-Senescent Potential

(A) Relative fractions of SA-β-gal-positive non-transgenic primary B-cells of the indicated genotypes 10 days after stable transduction with a Myc construct (≥ 80% of the cells infected; dead cells [around 40% initial apoptosis] were removed, resulting in about 5% senescent cells in the wild-type population) as compared to an empty vector.

(B) Growth parameters (*i.e.* Ki67, S-phase fraction by BrdU/PI [arrow], and SA-β-gal frequencies) in *bcl2*-infected non-transgenic B-cells (left) and Eμ-*myc*;*p53ER*$^{TAM/(-)}$/*bcl2* lymphoma lymphomas (right) in which functional p53 is restored in response to 4-OH-tamoxifen (4-OHT; solvent serving as the negative control) treatment for six days. Scale bar = 20 μm (identical magnification throughout the panel).

(C) Acute induction of functional p53 by administration of tamoxifen in mice bearing lymphomas as in (B); stained for BrdU labelling, Ki67 reactivity (H3K9me3: 10.7% ± 3.5 [solvent] *vs.* 39.0% ± 6.2 [tamoxifen]), apoptosis-indicating cleavage (cl.) of Caspase 3, and SA-β-gal activity. Scale bar = 50 μm (identical magnification throughout the panel).

(D) SA-β-gal frequencies in lymphomas as in (B) exposed *in vitro* for six days to 4-OHT (or a solvent as negative control) with no additional compound, or 5 mM of the ATM/ATR inhibitor caffeine (caf), 5 mM of the ROS scavenger N-acetyl-cysteine (NAC), or both.

At least three cases each in all these experiments; all numbers indicate the mean percentages of positive cells ± SD; "*" reflects $P < 0.05$. See also Figure S2.

Figure 3. TGF-β Induces Suv39h1-Dependent Cellular Senescence in Myc-Driven Lymphomas

(A) Focal TGF-β1 detected by immunostaining (left) and co-staining (right) for TGF-β1 (red) and Ki67 (blue) in control *vs. Suv39h1*$^{-}$ lymphomas in lymph node sections *in situ* (representative photomicrographs). Inserts show TGF-β1-rich areas at higher magnification, and percentages reflect the fraction Ki67-positive cells within those areas ($n = 3$ samples each). Scale bar = 50 μm (identical magnification throughout the panel).

(B) Growth curve analyses of freshly isolated and stably *bcl2*-infected control and *Suv39h1*$^{-}$ lymphoma cells exposed to the indicated concentrations of TGF-β1 (100 pM [red], 1000 pM [green]) or left untreated (black); $n = 5$ each. Inserts show untreated *vs.* TGF-β1-exposed (100 pM; day 5) lymphoma cell cytospin preparations assayed for SA-β-gal (top; 50.0% ± 13.2 [control] *vs*. 3.3% ± 2.9 [*Suv39h1*$^{-}$] for TGF-β1) and H3K9me3 reactivity (bottom; in red with DAPI as counterstain; 35.4% ± 14.4 [control] *vs.* 0.4% ± 0.1 [*Suv39h1*$^{-}$] for TGF-β1). Note the comparable proliferative capacities of Suv39h1-proficient and -deficient lymphoma cells in the absence of TGF-β1 treatment. Scale bar = 10 μm (identical magnification throughout the panel).

(C) Immunoblot analysis of Cyclin A protein levels (α-Tubulin as a loading control) in lymphomas as in (B) with or without preceding exposure to TGF-β1 (100 pM for 5 days).

(D) Relative growth of Bcl2-expressing lymphoma cells of the indicated genotypes after 5 days of exposure to TGF-β1 (100 pM) *vs.* untreated (as in [B]). At least three cases each.

Error bars denote the SD.; "*" reflects $P < 0.05$. See also Figure S3.

Figure 4. Environmental TGF-β, As Secreted by Apoptotic Lymphoma Cell-Activated Macrophages, Accounts For Lymphoma Cell Senescence *In Vivo*

(A) Relative induction of TGF-β1 protein levels at 48 hours by ELISA in cell culture supernatants of primary peritoneal macrophages (pMP) alone or after co-culture with Eμ-*myc*;*p53ER*$^{TAM/(-)}$ lymphomas exposed for 20 hours to 4-OHT or solvent ($n = 3$ each; relative to the normalized medium-corrected 'pMP solvent' value). Note that 4-OHT, but not solvent, quantitatively produced PS-positive apoptotic lymphoma cells

(Figure S4B). Relative induction of TGF-β1 secretion at 48 hours by PMA-stimulated (200 ng/ml) Ana-1 macrophages for comparison (in triplicate).

(B-D) Quantification of macrophage infiltration (Mac) measured by F4/80 immunostaining (numbers indicating average macrophage count per high-power field) and of senescence (Sen) assessed by SA-β-gal staining (B) in apoptosis-blocked Bcl2-expressing lymphomas, generated by retroviral *bcl2* transfer (or an empty vector as control) into Eμ-*myc* transgenic fetal liver cells and their subsequent propagation in lethally irradiated recipients, at manifestation, (C) following adoptive transfer of PMA-stimulated Ana-1 macrophages (as in [A]) by intravenous transfer into control lymphoma bearing mice, and (D) after systemic monocyte/macrophage depletion by liposome-encapsulated clodronate or empty liposomes for comparison.

(E) Tumor latencies, stratified by lymphoma GFP expression, in lethally irradiated recipients of Eμ-*myc* transgenic fetal liver cells stably transduced with the MSCV-TGF-β receptor type II ecto domain-IRES-GFP (TβR-II-ED/GFP) retrovirus (TβR-II-ED/GFP-positive, $n = 9$, green, *vs.* mock/GFP-negative, $n = 11$, black).

(F) Quantification of macrophage infiltration and senescence, assessed as in (B-D), in TβR-II-ED/GFP-expressing *vs.* mock-infected lymphomas as in (E). Note that around 10-20% of the overall senescence frequency can be attributed to the cell-autonomous component (see also [B]).

(G) Matched pair quantification of cellular senescence in individual control lymphomas ($n = 6$) infected with the TβR-II-ED/GFP or an empty/GFP retrovirus that formed after sorting and transplantation of GFP-expressing cells.

(H) Senescence frequencies of *bcl2*-infected control lymphoma cells exposed – in the presence or absence of the TGF-β receptor type I inhibitor SD-208 (TGFR-I; 500 nM) –

to pMP that were either native or co-cultivated with Eμ-*myc*;*p53ER*$^{TAM/(-)}$ lymphomas plus solvent or 4-OHT for 48 hours.

All experiments in this figure represent at least three independent samples each; all numbers indicate mean values ± SD; "*" reflects $P < 0.05$; "n.s." not significant. See also Figure S4.

Figure 5. Human Diffuse Large B-Cell Lymphomas (DLBCL) Display Features Consistent with the Model of Non-Cell-Autonomous TGF-β-Mediated Cellular Senescence

(A) Two DLBCL cases reflecting a highly (Ki67^{hi}; samples with ≥ 80% Ki67-positive cells) and a less intensely proliferating (Ki67^{lo}; samples with < 80% Ki67-positive cells) subgroup also stained for apoptosis (cleaved Caspase 3), macrophage infiltration (CD68), TGF-β pathway activation (*i.e.* Smad3-P), and cellular senescence (*i.e.* H3K9me3 as a surrogate marker). Representative photomicrographs of a total of 30 cases analyzed. Scale bar = 100 μm (identical magnification throughout the panel).

(B) Quantitative assessment of cleaved (cl.) Caspase 3, CD68, Smad3-P, and H3K9me3 in the Ki67 low *vs.* high groups (Ki67^{lo}, $n = 19$, Ki67 reactivity 68.7% ± 6.6 *vs.* Ki67^{hi}, $n = 11$, 88.9% ± 5.7; $P < 0.001$). All comparisons are highly statistically significant (*i.e.* $P < 0.001$), except a trend ($P = 0.07$) for cl. Caspase 3. All numbers indicate mean values ± SD; "*" reflects $P < 0.05$. Notably, no clear association of the Ki67 status with the germinal center (GC) B-cell-of-origin status (GCB *vs.* non-GCB by immunostaining (Hans et al., 2004), data not shown) was observed.

(C) Model of oncogene-initiated cell-autonomous and non-cell-autonomous cellular senescence in aggressive B-cell lymphomas, as concluded from Eμ-*myc* mouse lymphoma data.

Fig. 1

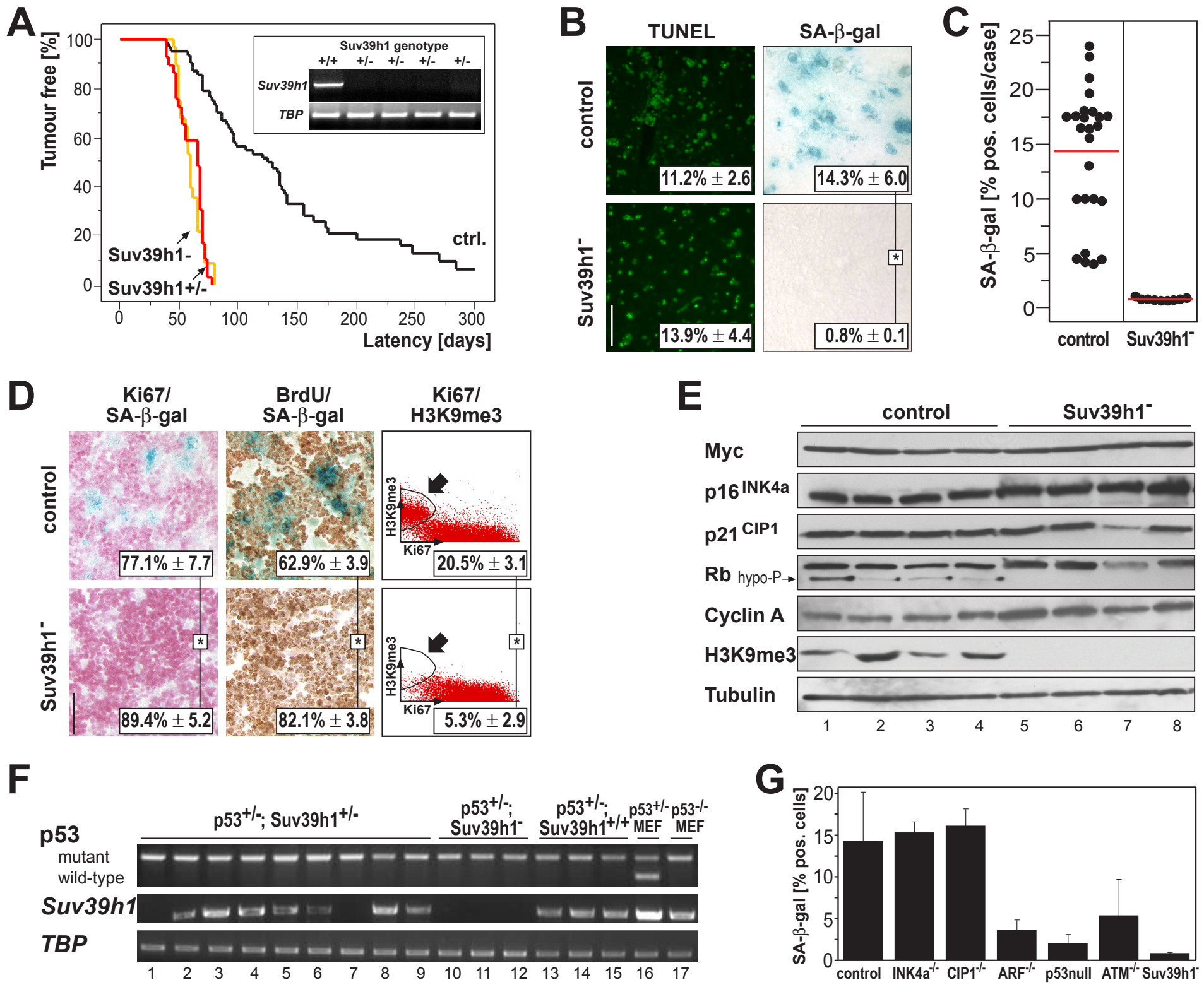
A
Tumour free [%]
Latency [days]
Suv39h1 genotype
+/+ +/- +/- +/- +/-
Suv39h1
TBP
Suv39h1-
Suv39h1+/-
ctrl.
B
TUNEL
SA-β-gal
control
Suv39h1-
11.2% ± 2.6
14.3% ± 6.0
13.9% ± 4.4
0.8% ± 0.1
C
SA-β-gal [% pos. cells/case]
control
Suv39h1-
D
Ki67/ SA-β-gal
BrdU/ SA-β-gal
Ki67/ H3K9me3
77.1% ± 7.7
62.9% ± 3.9
20.5% ± 3.1
89.4% ± 5.2
82.1% ± 3.8
5.3% ± 2.9
H3K9me3
Ki67
E
control
Suv39h1-
Myc
p16 INK4a
p21 CIP1
Rb hypo-P
Cyclin A
H3K9me3
Tubulin
F
p53+/-; Suv39h1+/-
p53+/- Suv39h1-
p53+/- Suv39h1+/+
p53+/- MEF
p53-/- MEF
p53
mutant
wild-type
Suv39h1
TBP
G
SA-β-gal [% pos. cells]
control
INK4a-/-
CIP1-/-
ARF-/-
p53null
ATM-/-
Suv39h1-

Fig. 2

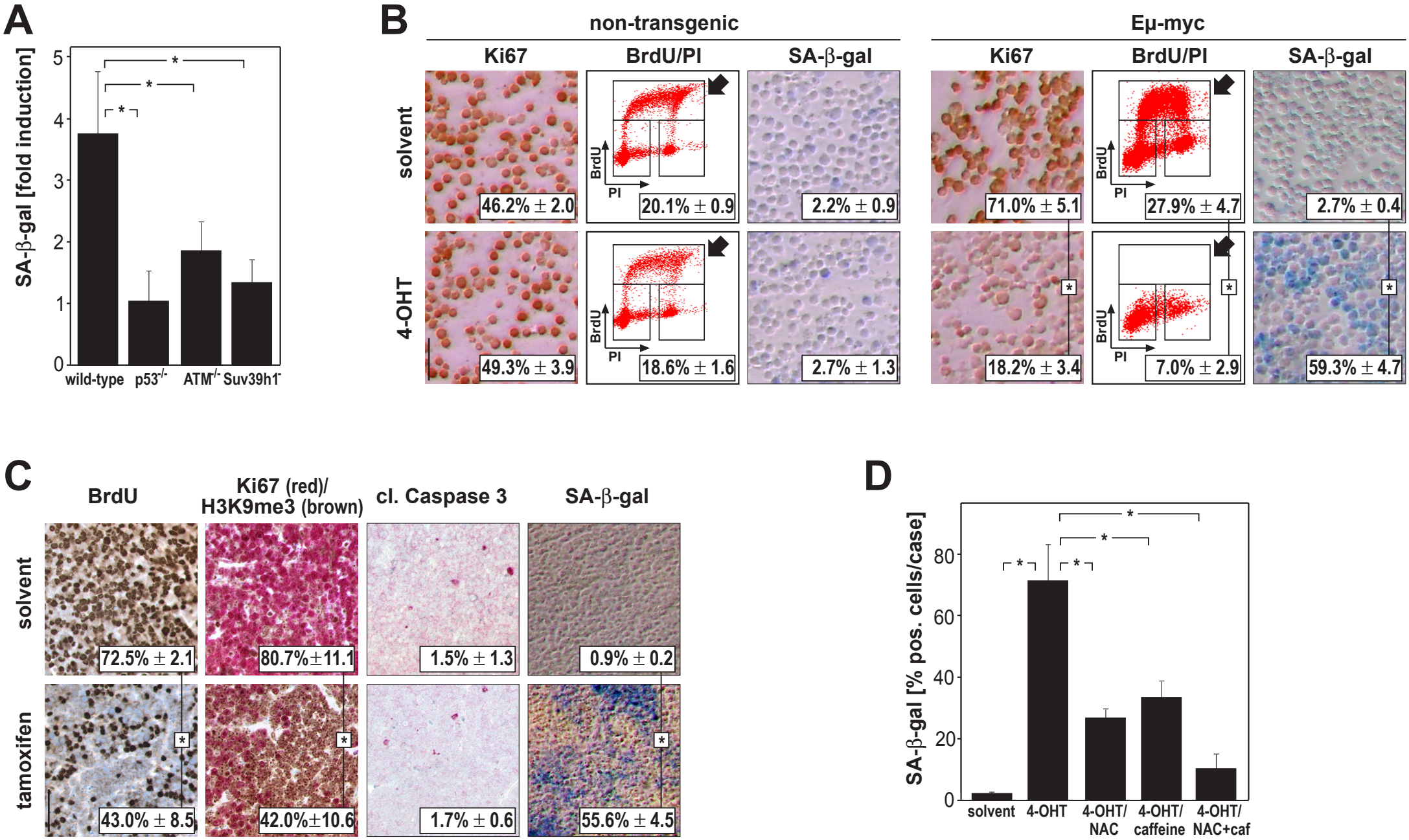
A
SA-β-gal [fold induction]
wild-type
p53-/-
ATM-/-
Suv39h1-
B
non-transgenic
Eμ-myc
Ki67
BrdU/PI
SA-β-gal
solvent
4-OHT
46.2% ± 2.0
20.1% ± 0.9
2.2% ± 0.9
71.0% ± 5.1
27.9% ± 4.7
2.7% ± 0.4
49.3% ± 3.9
18.6% ± 1.6
2.7% ± 1.3
18.2% ± 3.4
7.0% ± 2.9
59.3% ± 4.7
BrdU
PI
C
BrdU
Ki67 (red)/ H3K9me3 (brown)
cl. Caspase 3
SA-β-gal
solvent
tamoxifen
72.5% ± 2.1
80.7%±11.1
1.5% ± 1.3
0.9% ± 0.2
43.0% ± 8.5
42.0%±10.6
1.7% ± 0.6
55.6% ± 4.5
D
SA-β-gal [% pos. cells/case]
solvent
4-OHT
4-OHT/ NAC
4-OHT/ caffeine
4-OHT/ NAC+caf

Fig. 3

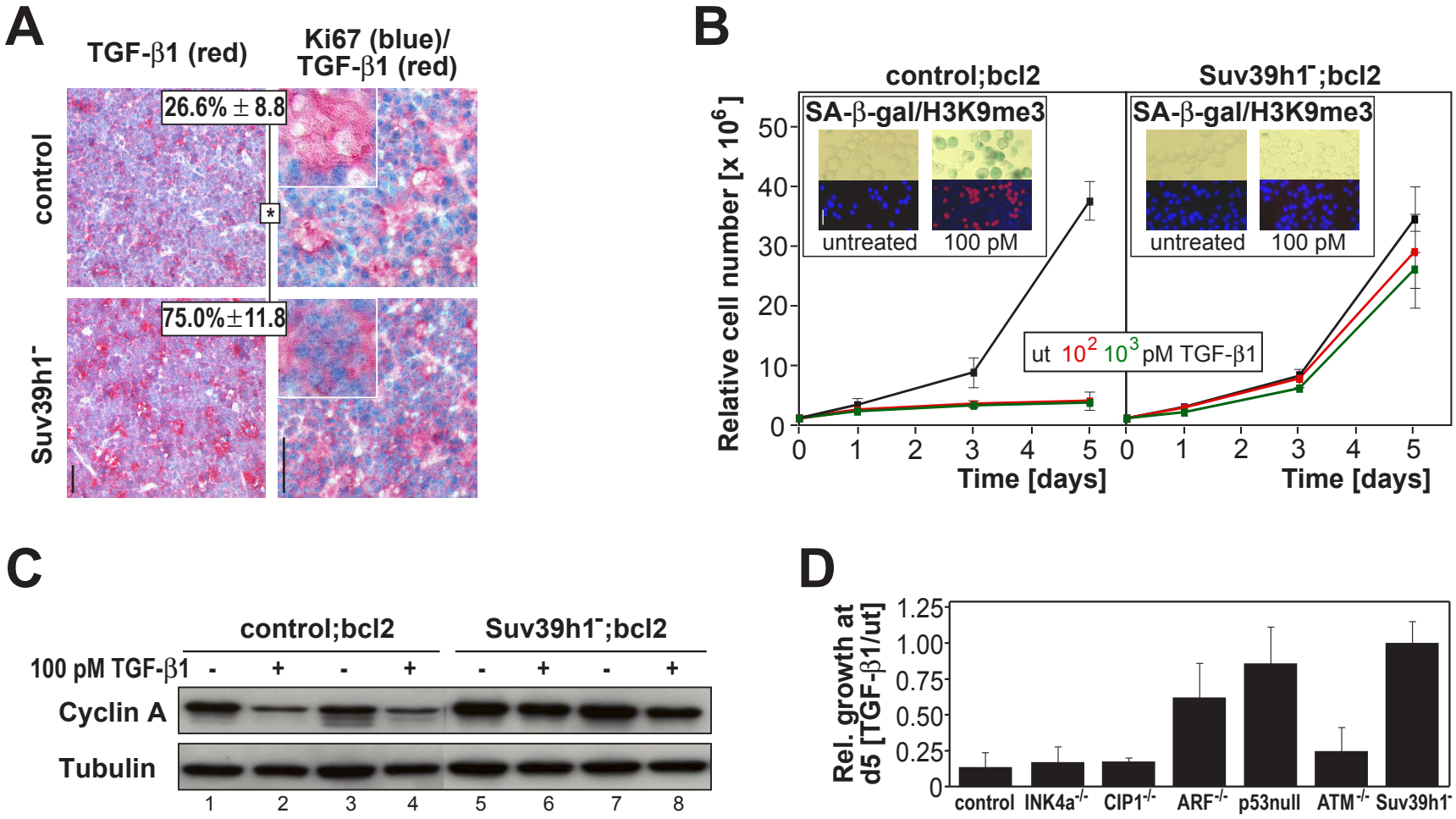
A
TGF-β1 (red)
Ki67 (blue)/
TGF-β1 (red)
control
Suv39h1-
26.6% ± 8.8
75.0%±11.8
*
B
control;bcl2
Suv39h1-;bcl2
SA-β-gal/H3K9me3
untreated
100 pM
Relative cell number [x 10^6]
Time [days]
ut 10^2 10^3 pM TGF-β1
C
control;bcl2
Suv39h1-;bcl2
100 pM TGF-β1
Cyclin A
Tubulin
D
Rel. growth at
d5 [TGF-β1/ut]
control
INK4a-/-
CIP1-/-
ARF-/-
p53null
ATM-/-
Suv39h1-

Fig. 4

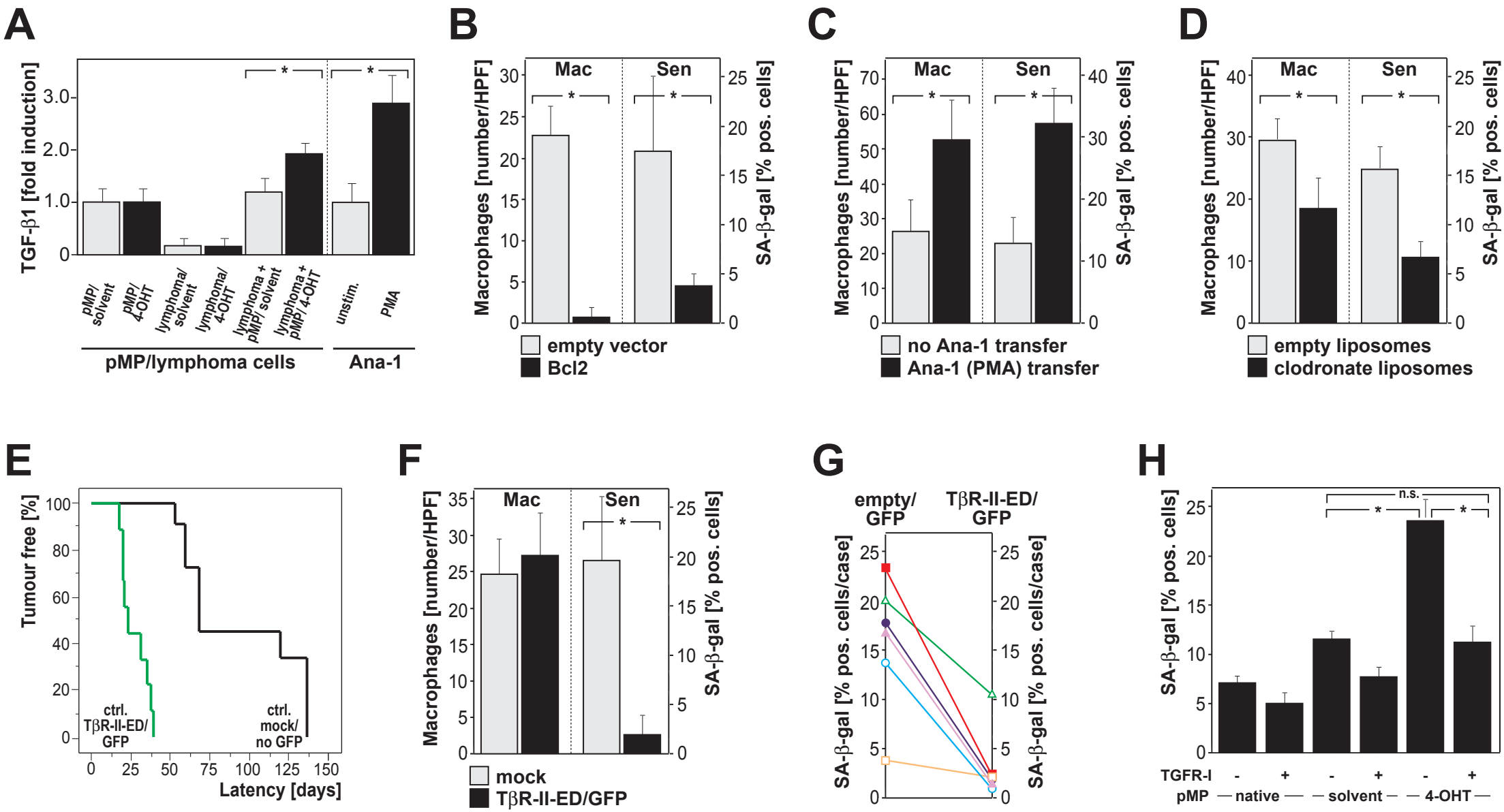
A
TGF-β1 [fold induction]
pMP/ solvent
pMP/ 4-OHT
lymphoma/ solvent
lymphoma/ 4-OHT
lymphoma + pMP/ solvent
lymphoma + pMP/ 4-OHT
unstim.
PMA
pMP/lymphoma cells
Ana-1
B
Macrophages [number/HPF]
SA-β-gal [% pos. cells]
Mac
Sen
empty vector
Bcl2
C
no Ana-1 transfer
Ana-1 (PMA) transfer
D
empty liposomes
clodronate liposomes
E
Tumour free [%]
Latency [days]
ctrl. TβR-II-ED/ GFP
ctrl. mock/ no GFP
F
mock
TβR-II-ED/GFP
G
empty/ GFP
TβR-II-ED/ GFP
SA-β-gal [% pos. cells/case]
H
n.s.
TGFR-I
pMP
native
solvent
4-OHT

Fig. 5

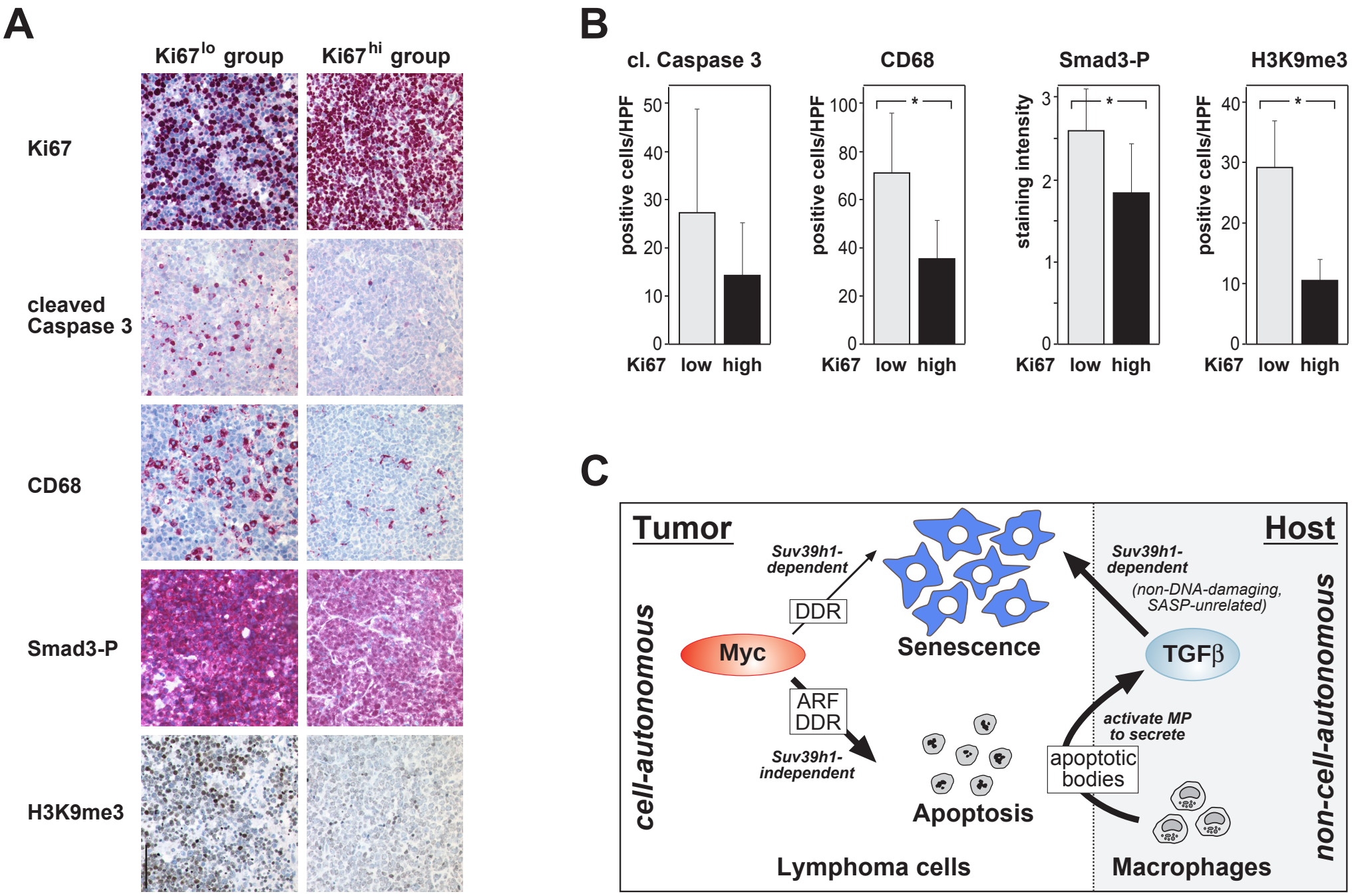
A
Ki67lo group
Ki67hi group
Ki67
cleaved Caspase 3
CD68
Smad3-P
H3K9me3
B
cl. Caspase 3
CD68
Smad3-P
H3K9me3
positive cells/HPF
staining intensity
Ki67 low high
*
C
Tumor
Host
cell-autonomous
non-cell-autonomous
Suv39h1-dependent
DDR
Myc
Senescence
ARF DDR
Suv39h1-independent
Apoptosis
Lymphoma cells
Suv39h1-dependent
(non-DNA-damaging, SASP-unrelated)
TGFβ
activate MP to secrete
apoptotic bodies
Macrophages

Supplemental Data

Tumor Stroma-Derived TGF-β Limits Myc-Driven Lymphomagenesis *via* Suv39h1-Dependent Senescence

Maurice Reimann[1,6], Soyoung Lee[1,2,6], Christoph Loddenkemper[3,6], Jan R. Dörr[1,6], Vedrana Tabor[2,6], Peter Aichele[4], Harald Stein[3], Bernd Dörken[1,2], Thomas Jenuwein[5], and Clemens A. Schmitt[1,2]

CONTENTS

SUPPLEMENTAL FIGURES

Fig. S1

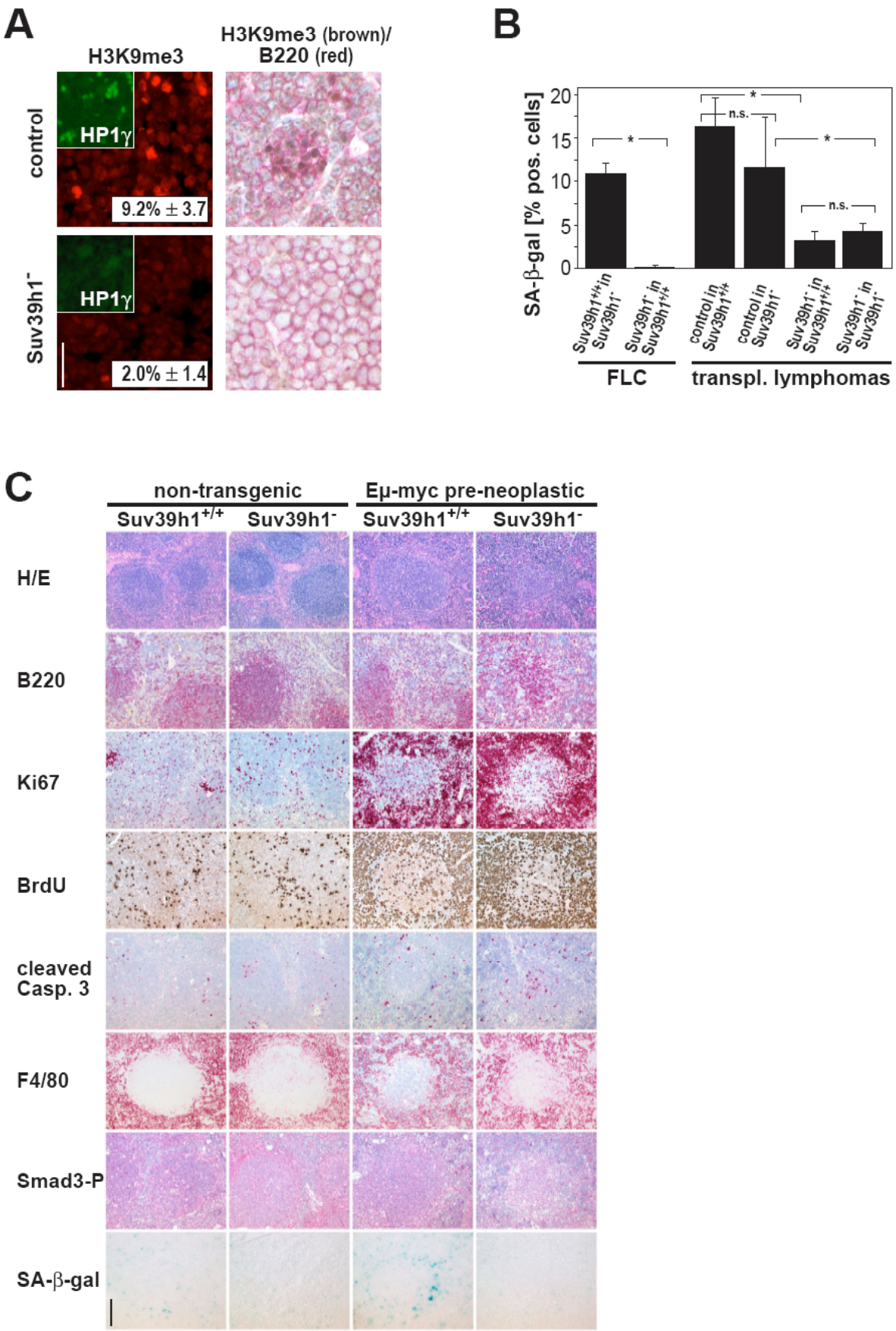
A
H3K9me3
H3K9me3 (brown)/
B220 (red)
control
Suv39h1-
HP1γ
9.2% ± 3.7
HP1γ
2.0% ± 1.4
B
SA-β-gal [% pos. cells]
20
15
10
5
0
*
n.s.
*
*
n.s.
Suv39h1+/+ in Suv39h1-
Suv39h1- in Suv39h1+/+
control in Suv39h1+/+
control in Suv39h1-
Suv39h1- in Suv39h1+/+
Suv39h1- in Suv39h1-
FLC
transpl. lymphomas
C
non-transgenic
Eμ-myc pre-neoplastic
Suv39h1+/+
Suv39h1-
Suv39h1+/+
Suv39h1-
H/E
B220
Ki67
BrdU
cleaved Casp. 3
F4/80
Smad3-P
SA-β-gal

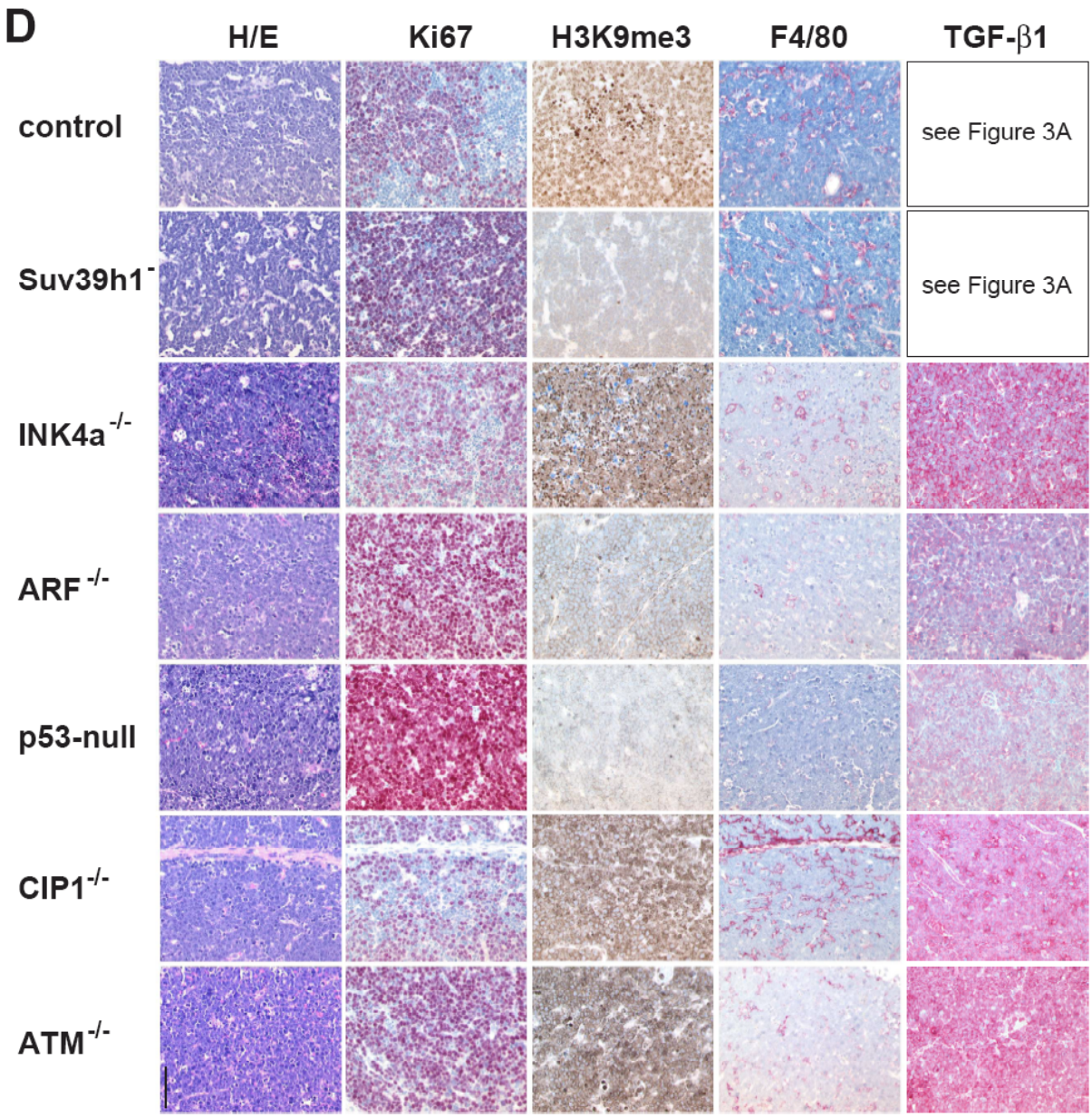

Figure S1. Analysis of Growth-Related Parameters in Non-Transgenic, Pre-neoplastic and Malignant Lymphoid Tissues of Mice with Defined Genetic Lesions. Related to Figure 1

(A) Immunofluorescence analyses of H3K9me3- and HP1γ-expressing (insert; control 14.1% ± 5.0; *Suv39h1*$^{-}$ 3.1% ± 1.3) cells, recapitulating the frequency of SA-β-gal-positive cells found in lymphoma sections *in situ* (left; compare to Figure 1B and 1C). Co-staining of the B-cell marker B220 (red) and H3K9me3 (brown) in lymph node sections of control and *Suv39h1*$^{-}$ lymphoma to verify the B-cell origin of the H3K9me3-reactive cells (right; representative photomicrographs of at least three cases each). Scale bar = 20 μm (identical magnification throughout the panel).

(B) SA-β-gal frequencies in lymphomas that formed upon propagation of Eμ-*myc Suv39h1*$^{+/+}$ fetal liver cells in sublethally irradiated non-transgenic *Suv39h1*$^{-}$ recipients, or, *vice versa*, of Eμ-*myc Suv39h1*$^{-}$ fetal liver cells (FLC) transplanted into non-transgenic *Suv39h1*$^{+/+}$ (*i.e.* wild-type) mice, as well as SA-β-gal analyses of Myc-lymphomas of the indicated genotypes transplanted at manifestation into either Suv39h1-proficient or -deficient recipient mice, supporting the view that lymphoma cells but not non-neoplastic bystanders comprise the fraction of SA-β-gal-positive cells. All numbers indicate the mean percentages of positive cells ± SD, measured in at least three independent samples; "*" reflects $P < 0.05$; "n.s." not significant.

(C) Representative photomicrographs of spleen samples obtained from *Suv39h1*$^{+/+}$ and *Suv39h1*$^{-}$ non-transgenic and Eμ-*myc* transgenic pre-neoplastic mice stained with hematoxylin/eosin (H/E) or assessed for the indicated markers *in situ*. Note the massive Myc-dependent but Suv39h1-independent peri-follicular proliferation and expansion of B-cells (by B220 and Ki67 immunostaining, and detection of BrdU incorporation) accompanied by a rather modest increase of apoptotic cells (as evidenced by cleaved Caspase 3) at this stage. Compared to the non-transgenic specimens, no Myc-related, additional infiltration of macrophages is observed above the substantial presence of red pulp-associated string macrophages (detected by F4/80 staining), which appear not to be activated to secrete increased amounts of TGF-β as there is no difference in the sparse pattern of Smad3-P-positive cells between non-transgenic and Eμ-*myc* pre-neoplastic samples (also compare to Figure S3J, demonstrating no detectable Smad3-P in bulk lysates of freshly isolated and immunobead-selected non-transgenic and pre-neoplastic B-cells by immunoblot analysis, while manifest lymphoma cells presented with intense Smad3-P signals). Importantly, a significant increase of SA-β-gal-positive peri-follicular cells became evident in *Suv39h1*$^{+/+}$ pre-neoplastic samples as compared to their rarity in the non-transgenic spleen, whereas *Suv39h1*$^{-}$ samples remained virtually negative for senescent cells independent of their Myc status. Scale bar = 200 μm (identical magnification throughout the panel).

(D) H/E staining and immunohistochemical analysis of markers reflecting proliferation (Ki67), cellular senescence (H3K9me3; compare to Figure 1G), and macrophage infiltration (F4/80) as well as TGF-β1 secretion in Eμ-*myc* transgenic lymphomas with defined genetic lesions. Note the virtual absence of H3K9me3 reactivity in the most uniformly Ki67-positive *Suv39h1*$^{-}$, *ARF*$^{-/-}$ and p53-null genotypes, with very low contents of lymphoma-infiltrating macrophages and low amounts of TGF-β1 *in situ* restricted to the apoptosis-compromised (Schmitt et al., 2002; Schmitt et al., 1999) ARF- and p53-deficient lymphoma genotypes, while no difference was found regarding the macrophage frequencies and TGF-β1 (see Figure 3A and Figure S3J) between control and *Suv39h1*$^{-}$ lymphomas. *ATM*$^{-/-}$ lymphomas, known to form with less apoptotic cells when compared to control lymphomas (Reimann et al., 2007), exhibit a slightly reduced degree of macrophage infiltration. Photomicrographs reflect representative samples of at least three individual lymphomas per genotype. Scale bar = 100 μm (identical magnification throughout the panel).

Fig. S2

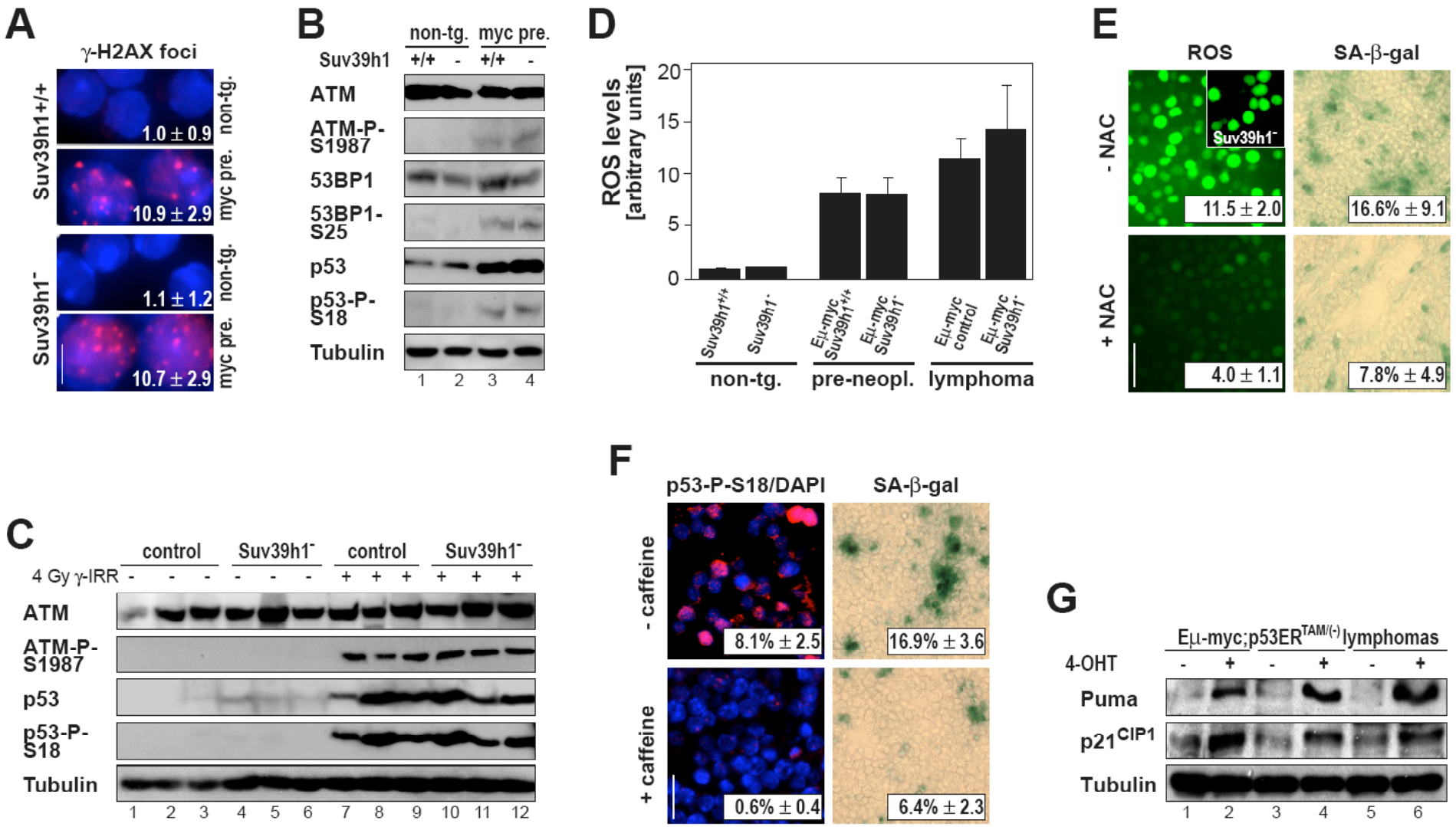
A
γ-H2AX foci
Suv39h1+/+
non-tg.
1.0 ± 0.9
myc pre.
10.9 ± 2.9
Suv39h1-
non-tg.
1.1 ± 1.2
myc pre.
10.7 ± 2.9
B
non-tg.
myc pre.
Suv39h1
+/+ - +/+ -
ATM
ATM-P-S1987
53BP1
53BP1-S25
p53
p53-P-S18
Tubulin
1 2 3 4
D
ROS levels [arbitrary units]
20
15
10
5
0
Suv39h1+/+
Suv39h1-
Eμ-myc Suv39h1+/+
Eμ-myc Suv39h1-
Eμ-myc control
Eμ-myc Suv39h1-
non-tg.
pre-neopl.
lymphoma
E
ROS
SA-β-gal
- NAC
Suv39h1-
11.5 ± 2.0
16.6% ± 9.1
+ NAC
4.0 ± 1.1
7.8% ± 4.9
C
control
Suv39h1-
control
Suv39h1-
4 Gy γ-IRR - - - - - - + + + + + +
ATM
ATM-P-S1987
p53
p53-P-S18
Tubulin
1 2 3 4 5 6 7 8 9 10 11 12
F
p53-P-S18/DAPI
SA-β-gal
- caffeine
8.1% ± 2.5
16.9% ± 3.6
+ caffeine
0.6% ± 0.4
6.4% ± 2.3
G
Eμ-myc;p53ER^TAM/(-) lymphomas
4-OHT - + - + - +
Puma
p21CIP1
Tubulin
1 2 3 4 5 6

Figure S2. The Oncogene-Evoked DDR and ROS Cell-Autonomously Drive Induction of Cellular Senescence. Related to Figure 2

(A) Quantification of γ-H2AX foci per cell by immunofluorescence in immunobead-selected non-transgenic (non-tg.) *vs.* constitutively Myc-expressing pre-neoplastic (myc pre.) splenic *Suv39h1*$^{+/+}$ and *Suv39h1*$^{-}$ B-cell preparations (n = 3 individual preparations each; numbers indicate the mean counts ± SD). Scale bar = 5 μm (identical magnification throughout the panel).

(B) Immunoblot analyses of the indicated DDR components in lysates of B-cell preparations as in (A); α-Tubulin as a loading control. (C) Immunoblot analyses of the indicated DDR components in control *vs. Suv39h1*$^{-}$ lymphoma cells (n = 3 individual samples each) with or without preceding γ-irradiation (2 hours after 4 Gy); α-Tubulin as a loading control.

(D) 2'-7'-Dichlorodihydrofluorescein diacetate-based flow cytometric analysis of cellular ROS levels in freshly isolated and immunobead-selected B-cells demonstrate that no significant differences exist between Suv39h1-proficient and -deficient cells of the respective stages (n = 3 individual preparations each). All numbers indicate mean values ± SD.

(E) Cellular ROS levels (left; measured as in [D] by flow cytometry; representative photomicrographs of cytospin preparations by fluorescence microscopy) and corresponding SA-β-gal staining (right) of control lymphoma sections at manifestation after life-long exposure to N-acetyl-cysteine (+ NAC) or mock treatment (– NAC). Numbers indicate mean cellular ROS levels (insert: ROS level in untreated *Suv39h1*$^{-}$ lymphoma cells; 14.3 ± 4.2) or percentage of positive cells (SA-β-gal) ± SD obtained from at least five samples each. Scale bar = 20 μm (identical magnification throughout the panel).

(F) Quantification of p53-P-Ser18 by immunofluorescence (left) and corresponding SA-β-gal staining (right) in control lymphomas isolated at manifestation after life-long exposure to the ATM/ATR inhibitor caffeine or mock treatment. Numbers indicate the percentage of cells with positive nuclear staining (with respect to p53-P-Ser18) ± SD (representative

photomicrographs from at least five samples each); "*" reflects $P < 0.05$. Scale bar = 20 μm (identical magnification throughout the panel).

(G) Biochemical characteristics of Eμ-*myc* transgenic lymphomas carrying an inducible *p53* allele: immunoblot analyses of the p53 targets Puma and $p21^{CIP1}$ in lysates of three Eμ-*myc*;*p53ER*$^{TAM/(-)}$ lymphoma samples with and without exposure to 4-OHT (which also resulted in p53ER shuttling to the nucleus as confirmed by anti-ER immunofluorescence [data not shown]). Notably, p53 restoration is sufficient to drive $p21^{CIP1}$ expression despite constitutive Myc expression (as seen in response to DNA damage (Schmitt et al., 1999)), although Myc has been shown to selectively inhibit p53 from activating *CIP1* translation in other settings (Seoane et al., 2002).

Fig. S3

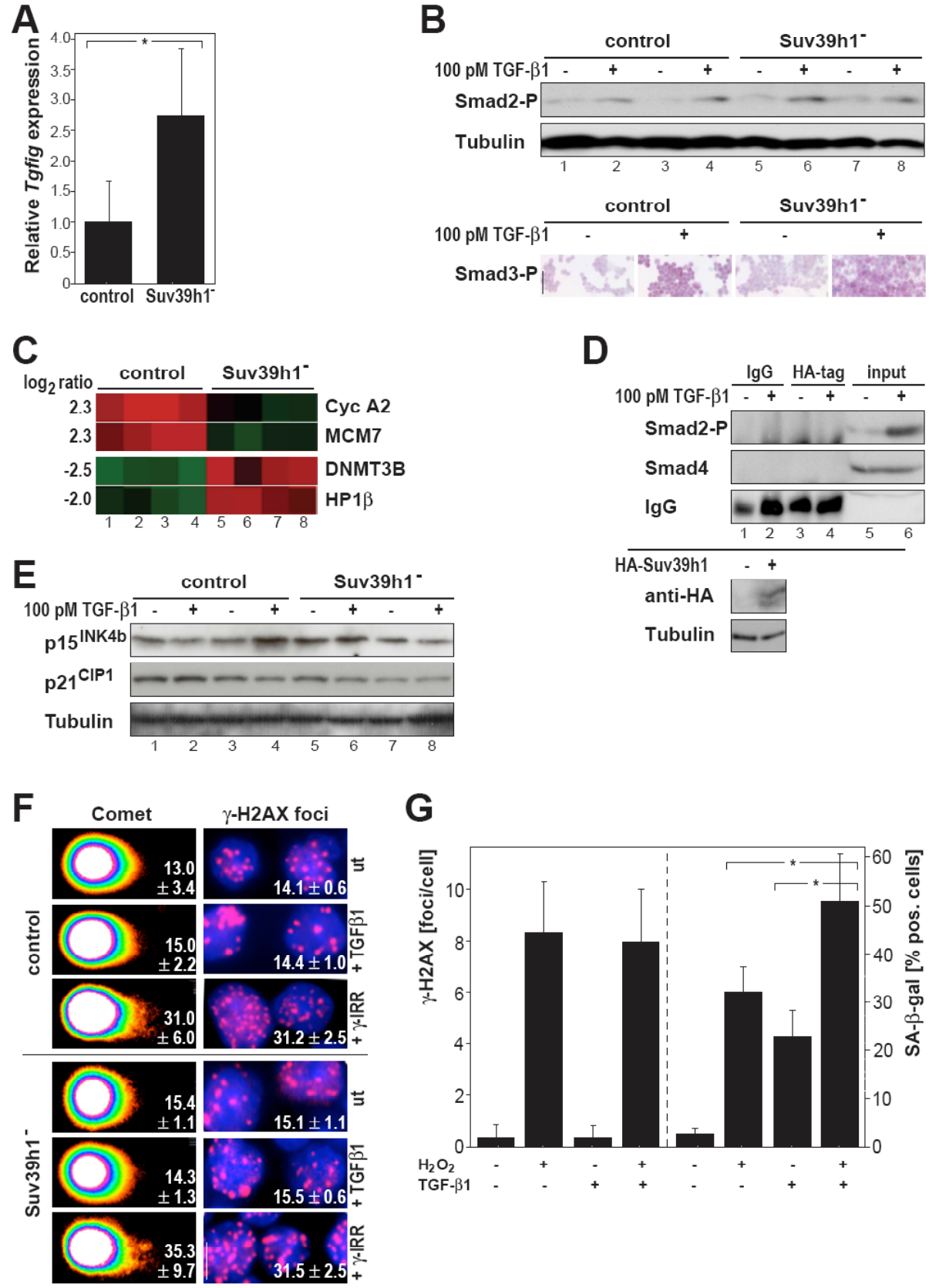
A
Relative Tgfig expression
4.0
3.5
3.0
2.5
2.0
1.5
1.0
0.5
0
*
control
Suv39h1-
B
control
Suv39h1-
100 pM TGF-β1 - + - + - + - +
Smad2-P
Tubulin
1 2 3 4 5 6 7 8
control
Suv39h1-
100 pM TGF-β1 - + - +
Smad3-P
C
log2 ratio
control
Suv39h1-
2.3
2.3
-2.5
-2.0
Cyc A2
MCM7
DNMT3B
HP1β
1 2 3 4 5 6 7 8
D
IgG
HA-tag
input
100 pM TGF-β1 - + - + - +
Smad2-P
Smad4
IgG
1 2 3 4 5 6
HA-Suv39h1 - +
anti-HA
Tubulin
E
control
Suv39h1-
100 pM TGF-β1 - + - + - + - +
p15INK4b
p21CIP1
Tubulin
1 2 3 4 5 6 7 8
F
Comet
γ-H2AX foci
control
Suv39h1-
13.0 ± 3.4
14.1 ± 0.6
ut
15.0 ± 2.2
14.4 ± 1.0
+ TGFβ1
31.0 ± 6.0
31.2 ± 2.5
+ γ-IRR
15.4 ± 1.1
15.1 ± 1.1
ut
14.3 ± 1.3
15.5 ± 0.6
+ TGFβ1
35.3 ± 9.7
31.5 ± 2.5
+ γ-IRR
G
γ-H2AX [foci/cell]
SA-β-gal [% pos. cells]
10
8
6
4
2
0
60
50
40
30
20
10
0
*
*
H2O2 - + - + - + - +
TGF-β1 - - + + - - + +

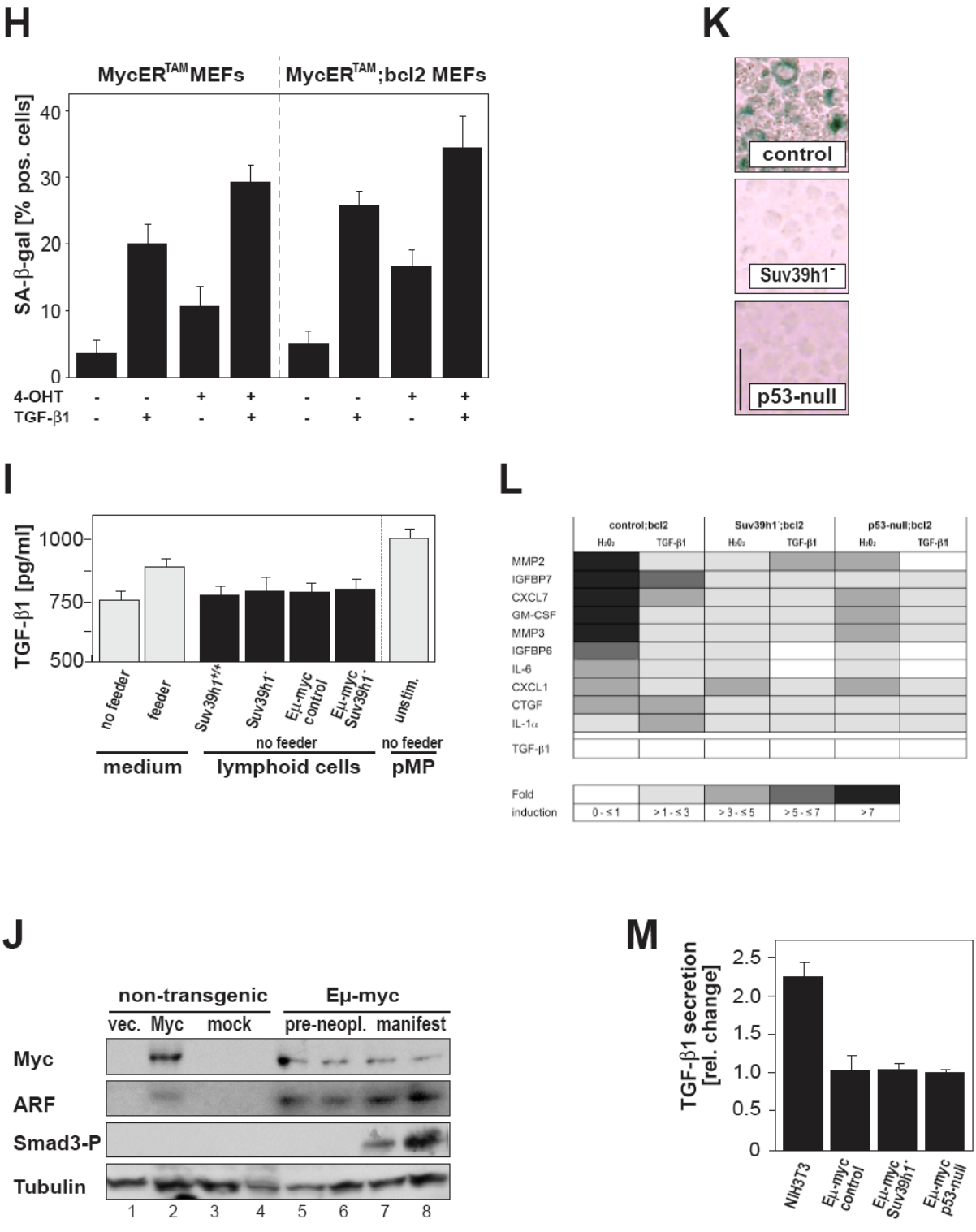
H
MycER^TAM MEFs
MycER^TAM;bcl2 MEFs
SA-β-gal [% pos. cells]
40
30
20
10
0
4-OHT - - + + - - + +
TGF-β1 - + - + - + - +
K
control
Suv39h1-
p53-null
I
TGF-β1 [pg/ml]
1000
750
500
no feeder
feeder
Suv39h1+/+
Suv39h1-
Eμ-myc control
Eμ-myc Suv39h1-
unstim.
medium
no feeder
lymphoid cells
no feeder
pMP
L
control;bcl2
Suv39h1-;bcl2
p53-null;bcl2
H2O2
TGF-β1
MMP2
IGFBP7
CXCL7
GM-CSF
MMP3
IGFBP6
IL-6
CXCL1
CTGF
IL-1α
TGF-β1
Fold induction
0 - ≤ 1
> 1 - ≤ 3
> 3 - ≤ 5
> 5 - ≤ 7
> 7
J
non-transgenic
Eμ-myc
vec.
Myc
mock
pre-neopl.
manifest
Myc
ARF
Smad3-P
Tubulin
1 2 3 4 5 6 7 8
M
TGF-β1 secretion [rel. change]
2.5
2.0
1.5
1.0
0.5
0
NIH3T3
Eμ-myc control
Eμ-myc Suv39h1-
Eμ-myc p53-null

Figure S3. TGF-β Signaling in Myc-Driven Lymphomas. Related to Figure 3

(A) Relative abundance of *Tgfbi* transcripts (as identified by microarray expression analysis; see "Experimental Procedures" section for details) by quantitative RT-PCR (RQ-PCR) analysis in freshly isolated immunobead-selected B-cell samples of *Suv39h1*$^-$ lymphomas compared to normalized levels in control lymphomas (n = 3 individual lymphomas each).

(B) Expression of phosphorylated Smad2 protein (Smad2-P) by immunoblot analysis (top) and of Smad3-P by immunocytochemical analysis (bottom) in two samples of control and *Suv39h1*$^-$ lymphoma cells treated with 100 pM TGF-β1 for 24 hours or left untreated; α-Tubulin as a loading control. Scale bar = 50 μm (identical magnification throughout the panel).

(C) Relative transcript abundances (visualized as heat-map [red: down, green: up] and $\log_2$ ratio [*Suv39h1*$^-$/control]) of selected differentially regulated genes in control and *Suv39h1*$^-$ lymphomas exposed to 100 pM TGF-β1 for 24 hours *in vitro* (n = 4 each).

(D) No detectable interaction of Suv39h1 with Smad2-P or Smad4 in lysates from TGF-β1-treated (100 pM for 6 hours) or untreated mouse embryo fibroblasts (MEF) stably expressing hemagglutinin (HA)-tagged Suv39h1 by immunoprecipitation with antibodies against IgG or the HA-tag followed by immunoblot analysis for the respective Smad proteins (top); confirmation of HA-Suv39h1 protein expression in infected MEF (bottom); α-Tubulin as a loading control.

(E) $p15^{INK4b}$ and $p21^{CIP1}$ expression by immunoblot analysis in control and *Suv39h1*$^-$ lymphomas exposed to 100 pM TGF-β1 for 24 hours *in vitro* or left untreated. α-Tubulin as a loading control. Of note, p53- and TGF-β-responsive elements and Miz-1 binding sites map to different regions of the *CIP1* promoter (Seoane et al., 2002), which may explain, at least in part, the different $p21^{CIP1}$ responses to TGF-β treatment as compared to p53 reactivation (Figure S2G) in Myc-driven lymphomas.

(F) Marks of DNA damage following TGF-β1 treatment (100 pM for 20 hours) *vs.* untreated (ut) by quantification of Comet mean tail moments and of γ-H2AX foci in Annexin V-negative control and *Suv39h1*$^{-}$ lymphomas; samples two hours after γ-irradiation (10 Gy for Comet, 4 Gy for γ-H2AX foci) as internal control (*n* = 3 samples each). Scale bar = 5 μm (identical magnification throughout the panel).

(G) Marks of DNA damage as measured by γ-H2AX foci/cell (left) and cellular senescence as analyzed by SA-β-gal staining (right) in LPS-stimulated, apoptosis-blocked Eμ-*bcl2* transgenic (but not Eμ-*myc* transgenic) B-lymphocytes (Strasser et al., 1990) at day 7 after treatments with either H_20_2 (100 μM), TGF-β1 (100 pM) or both or no treatment (*n* = 3 individual lymphocyte preparations each).

(H) Cellular senescence as analyzed by SA-β-gal staining in MycER^{TAM} MEFs – in which Myc is inactive in the absence of 4-OHT – with (right) or without (left) a Bcl2-mediated apoptotic block at day 7 after treatments with either 4-OHT (1 μM) or TGF-β1 (100 pM) or both or no treatment/solvent only (*n* = 3 individual MEF preparations each). Note that TGF-β is capable of inducing senescence in the absence of activated Myc.

(I) Absolute TGF-β1 concentrations by ELISA in cell culture media/supernatants of the indicated scenarios; unstimulated primary peritoneal macrophages (pMP) for comparison (*n* = 3 each). Of note, additional RQ-PCR analyses of short-term cultured lymphoma cells found transcript levels of TGF-β2 and TGF-β3 at even lower levels than TGF-β1-encoding transcripts in both control and *Suv39h1*$^{-}$ genotypes (data not shown), indicating that none of the TGF-β forms is expressed in Eμ-*myc* transgenic B-cell lymphoma cells.

(J) Myc, ARF and Smad3-P protein expression (with α-Tubulin as a loading control) in lysates from non-transgenic B-cells infected with a Myc-encoding, an empty (vec.) or no (mock) retrovirus as compared to freshly isolated and B-cell-immunobead-selected Eμ-*myc* transgenic pre-neoplastic or manifest control lymphoma cells, respectively. Note that ARF expression is expectedly tightly related to Myc expression, but constitutively Myc-(over)-expressing non-transgenic or pre-neoplastic B-cells do not display TGF-β pathway activation,

as reflected by lack of Smad3-P expression. Given the observation that some Eμ-*myc* transgenic B-cells already exhibited signs of cellular senescence at the pre-neoplastic state without displaying a parallel increment of Smad3-P-positive cells (Figure S1C), it seems conceivable that early SA-β-gal-positive lesions rather senesced due to a cell-autonomous Myc-evoked DDR.

(K) Senescence induction in lymphoma cells of the indicated genotypes exposed to an H_2O_2 (100 μM) pulse treatment for two hours and stained for SA-β-gal activity on day 5; shown are representative photomicrographs. Scale bar = 20 μm (identical magnification throughout the panel).

(L) Relative abundances of the indicated cytokine transcripts measured by RQ-PCR in *bcl2*-infected lymphomas of various genotypes at day 5 following pulse treatments with either H_2O_2 (100 μM for two hours as in [K]) or TGF-β1 (100 pM for six hours) as compared to untreated samples of the same genotype (n = 5 for control and *Suv39h1*$^-$; n = 3 for p53-null). Cytokine listing is ranked by induction levels upon H_2O_2 in control;bcl2 lymphoma cells.

(M) Relative changes of TGF-β1 concentrations by ELISA in cell culture supernatants of NIH3T3 fibroblasts and *bcl2*-infected lymphoma cells of the indicated genotypes five days after senescence-inducing doses (6 Gy) of γ-irradiation *vs.* no treatment (n = 3 individual lymphoma preparations each; NIH3T3 fibroblasts in triplicate; background levels subtracted). Note that only fibroblasts but not lymphoma cells (including senescence-capable control lymphoma cells) exhibited a significant increase of TGF-β1 secretion following therapy (similar data were obtained for H_2O_2 treatment; data not shown).

All numbers in this Figure indicate mean values ± SD; "*" reflects $P < 0.05$.

Fig. S4

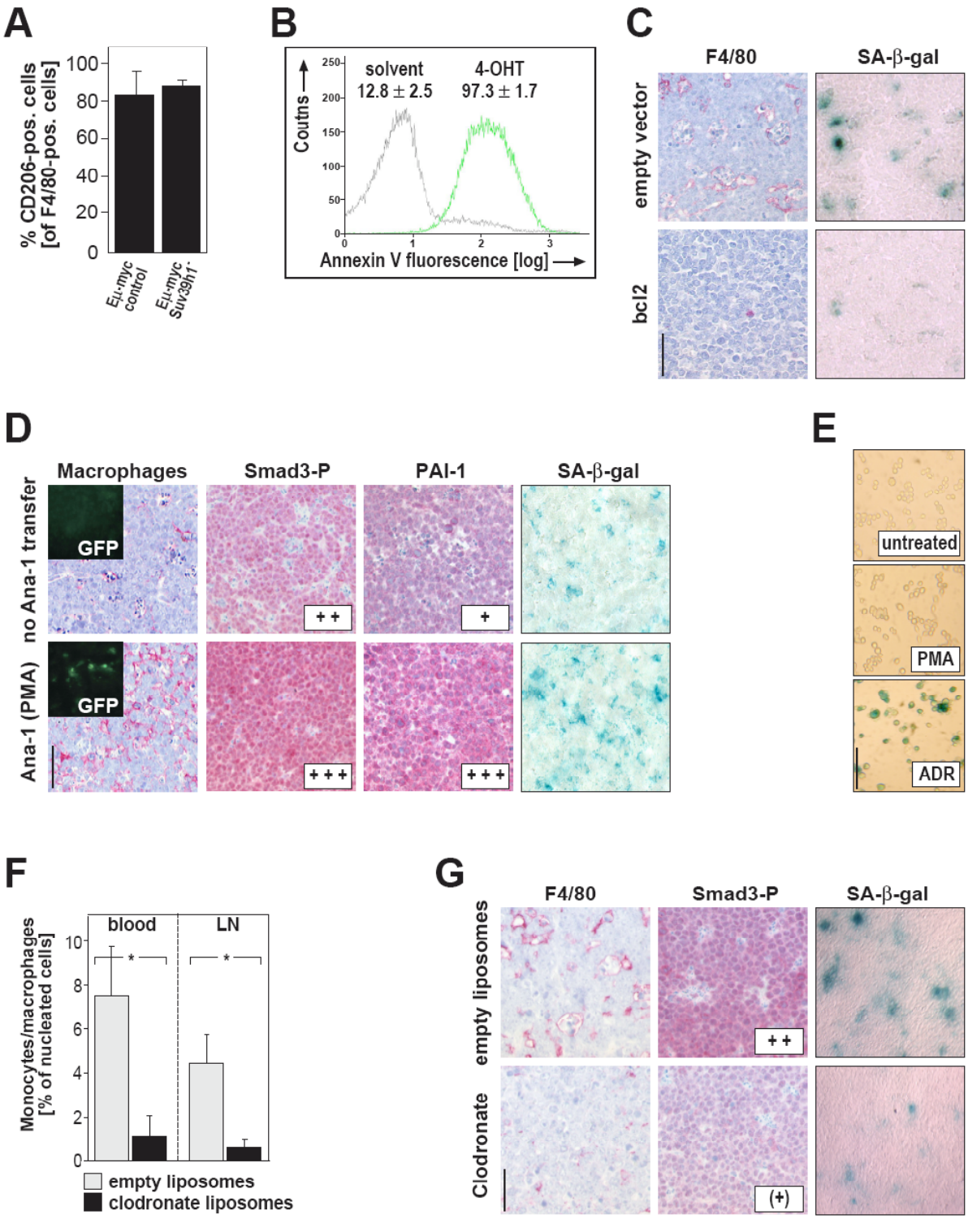
A
% CD206-pos. cells [of F4/80-pos. cells]
100
80
60
40
20
0
Eμ-myc control
Eμ-myc Suv39h1-
B
Counts
250
200
150
100
50
0
solvent
12.8 ± 2.5
4-OHT
97.3 ± 1.7
0
1
2
3
Annexin V fluorescence [log]
C
F4/80
SA-β-gal
empty vector
bcl2
D
Macrophages
Smad3-P
PAI-1
SA-β-gal
no Ana-1 transfer
Ana-1 (PMA)
GFP
GFP
++
+
+++
+++
E
untreated
PMA
ADR
F
Monocytes/macrophages [% of nucleated cells]
blood
LN
10
8
6
4
2
0
*
*
empty liposomes
clodronate liposomes
G
F4/80
Smad3-P
SA-β-gal
empty liposomes
Clodronate
++
(+)

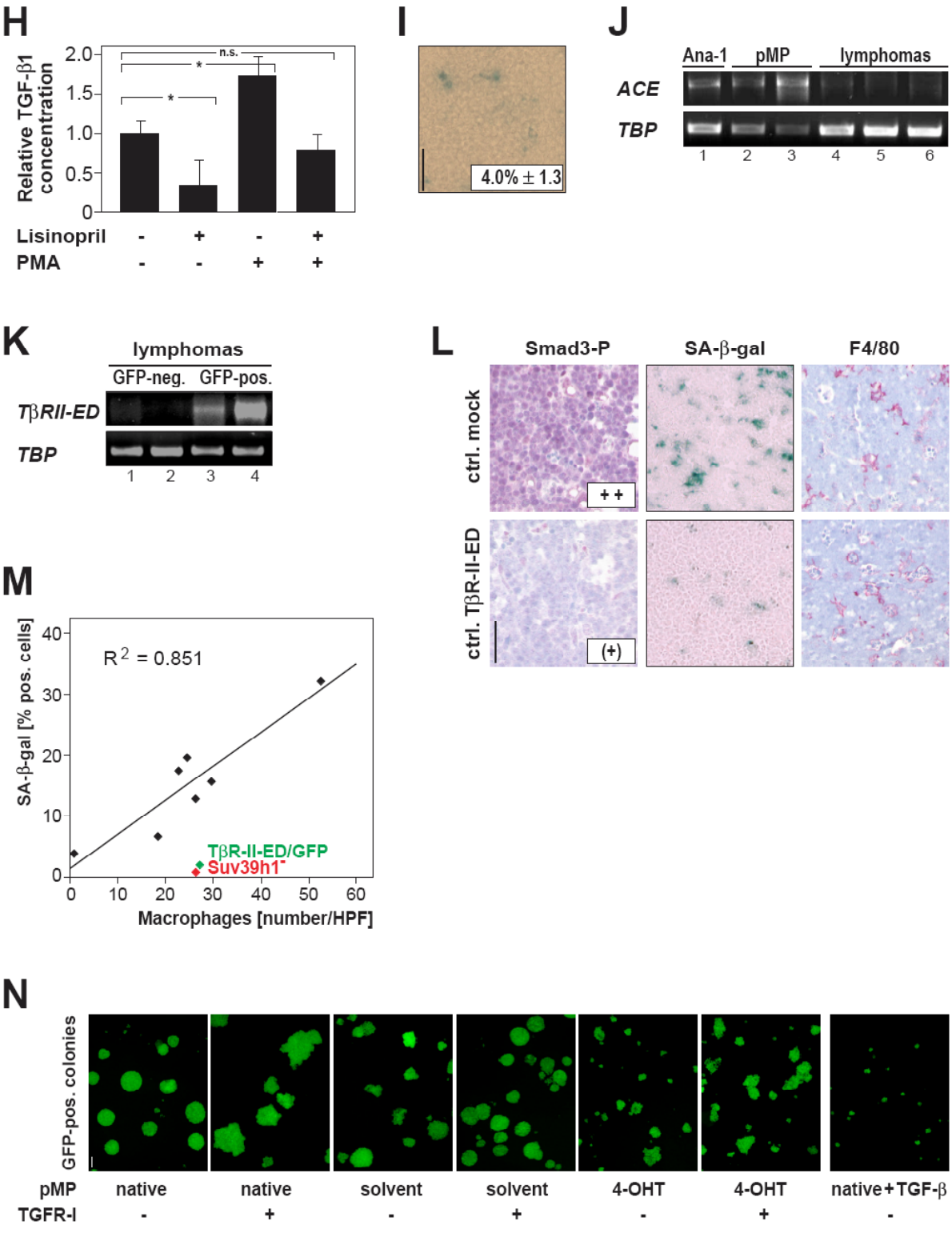

Figure S4. Characterization of The Lymphoma Cell Apoptosis/ Lymphoma-Infiltrating Macrophages/ TGF-β Secretion Cascade Into Senescence. Related to Figure 4

(A) Immunophenotyping of whole lymph node cell isolates from control *vs. Suv39h1*$^{-}$ lymphoma samples by flow cytometry assigns lymphoma-infiltrating macrophages

independent of the lymphoma genotype to the "M2 type", *i.e.* CD206-positive, tumor-associated macrophages that are known to serve as a source of TGF-β1 (Mantovani et al., 2002) (n = 5 individual lymphoma preparations each; presented is the fraction of CD206-positive cells within the F4/80-positive macrophage population).

(B) Apoptosis-related phosphatidylserine externalization detected by Annexin V flow cytometric staining of Eμ-*myc*;*p53ER*$^{TAM/(-)}$ lymphomas exposed to solvent or 4-OHT (1 μM for 24 hours; representative plot of n = 3 individual lymphomas). Note the quantitative apoptosis induction 24 hours after exposure to 4-OHT, as compared to an increase of around 6% apoptotic cells detectable in non-transgenic *p53ER*$^{TAM/(-)}$ cells (data not shown).

(C) Senescence reflected by SA-β-gal staining and assessment of macrophage infiltration by F4/80 immunostaining in apoptosis-blocked Bcl2-expressing lymphomas, generated by retroviral *bcl2* transfer (or an empty vector as control) into Eμ-*myc* transgenic fetal liver cells and their subsequent propagation in lethally irradiated recipients, at manifestation (n = 3 samples each). Representative photomicrographs related to the data set in Figure 4B.

(D) Adoptive transfer of GFP-transduced and PMA-stimulated (as in Figure 4A) Ana-1 macrophages by intravenous injection into control lymphoma-bearing mice. Macrophage infiltration of lymphoma sites by GFP (insert) and F4/80 immunostaining (red); TGF-β pathway activation by immunostaining for Smad3-P and PAI-1 *in situ*; senescence by SA-β-gal staining (six days after macrophage transfer). Representative photomicrographs of at least three cases each

(E) Ana-1 macrophages are senescent (as indicated by SA-β-gal staining) at day 7 following exposure to adriamycin (ADR; 0.2 μg/ml) but not to PMA (as in [D]); therefore, PMA-exposed macrophages do not account for increased frequencies of SA-β-gal-positive cells *in situ* following adoptive transfer. Scale bar = 20 μm (identical magnification throughout the panel).

(F) Monocyte/macrophage cell counts by 2-colour flow cytometric analysis (using antibodies against CD11b and F4/80) of peripheral blood samples and lymph node preparations of

normal wild-type mice 24 hours after intravenous injection of either empty liposomes or liposome-encapsulated clodronate.

(G) Macrophage infiltration of lymphoma sites by F4/80 immunostaining; TGF-β pathway activation by immunostaining for Smad3-P *in situ*; senescence by SA-β-gal staining. Representative photomicrographs of at least three cases each.

(H) Relative TGF-β1 protein levels (compared to normalized medium-corrected values of untreated pMP) by ELISA in cell culture supernatants of pMP exposed to PMA and to the *angiotensin-converting enzyme* (*ACE*) inhibitor lisinopril, which reportedly suppresses TGF-β1 production (Kagami et al., 1994). pMPs were pre-incubated for six hours with lisinopril (100 μM), PMA (200 ng/ml), or both, or medium only, washed and then exposed to PMA or left untreated for another 48 hours prior to ELISA; lisinopril was re-added at 24 hours (data shown reflect triplicates).

(I) Quantification of senescence by SA-β-gal staining in lymphomas arising in mice that were continuously exposed to lisinopril starting from about four weeks of age (n = 4 individual mice). Compared to untreated control lymphomas (Figure 1B), lisinopril treatment significantly reduced the frequency of SA-β-gal-positive cells in lymphomas at manifestation.

(J) Detection of *ACE* transcripts by RT-PCR in macrophages (Ana-1 cells and two independent pMP preparations), but not in lymphoma cells (Koca et al., 2007) (n = 3; with *TBP* as an internal control), indicating that lisinopril exerts its inhibitory function in macrophages, while lymphoma cells do not express the target enzyme.

(K) Detection of *TβR-II-ED* transcripts by RT-PCR in GFP-positive, but not in GFP-negative (as assessed by flow cytometry, data not shown) lymphoma samples derived from the TβR-II-ED/GFP-transduced FLC transplantation experiment (Figure 4E); shown are two representative cases each (with *TBP* as an internal control).

(L) TGF-β pathway activation analyzed by immunohistochemical staining for Smad3-P, and frequency of senescent cells by SA-β-gal staining in lymph node sections obtained at

manifestation from TβR-II-ED/GFP-positive *vs.* negative (mock) control lymphomas as in Figure 4E; note that macrophage infiltration (by F4/80 staining) remained unchanged (representative photomicrographs from at least three samples per genotype tested).

(M) Curve fitting analysis of the mean frequencies of lymphoma-infiltrating macrophages and of the corresponding mean SA-β-gal-positive cells (as shown in Figure 1B and 1C, Figure 4 and Figure S1D); *i.e.* calculated from the data points (black diamonds) referring to *bcl2* infection *vs.* empty vector, Ana-1 macrophage transfer *vs.* no transfer, clodronate treatment *vs.* empty liposomes, and mock infection as compared to the corresponding TβR-II-ED/GFP infection (green diamond) and as compared to *Suv39h1*$^{-}$ lymphomas (red diamond). Note the high coefficient of determination (R^2) for the fitted black coordinates as opposed by the outlier positions of the scenarios depicted in green and red, respectively.

(N) Apoptotic body-induced macrophage-derived TGF-β secretion suppresses lymphoma cell colony formation: matching the SA-β-gal frequencies measured in the respective single cell preparations of the colonies presented here (as shown in Figure 4H), GFP-positive control;bcl2 lymphoma cells co-cultured with primary peritoneal macrophages (pMP) in semi-solid methylcellulose formed less and on average much smaller colonies when pMP were pre-activated by 4-OHT-apoptotic Eμ-*myc*;*p53ER*$^{TAM/(-)}$ lymphoma cells (as compared to solvent-treated lymphoma cells or to native pMP that were not pre-exposed to lymphoma cells). Importantly, the observed growth suppression was largely prevented by co-incubation with the TGF-β receptor type I inhibitor SD-208 (TGFR-I; 500 nM). Note that some larger colonies in the 4-OHT/no TGFR-I setting may have escaped TGF-β-mediated growth suppression by rapid expansion out of the close proximity to adjacent macrophages, and, thus, potentially out of their senescence-effective TGF-β gradient. Experimental conditions with native pMP and exogenous addition of TGF-β1 (100 pM) are provided as an additional control for comparison. Shown are representative fluorescence micrographs of three independent experiments.

All numbers indicate the mean values ± SD; "*" reflects $P < 0.05$; "n.s." not significant. All scale bars in this figure represent 50 μm.

SUPPLEMENTAL EXPERIMENTAL PROCEDURES

In vivo-Treatments

In some experiments, mice were exposed to the following drug treatments until lymphomas were harvested: 5-bromo-2'-deoxyuridine (BrdU, 100 mg/kg, supplemented with 10 mg/kg 5-fluoro-2'-deoxyuridine [FDU]; BrdU *in situ* detection kit, BD Pharmingen) administered intraperitoneally (*i.p.*) 24 hours prior to lymphoma isolation, or 1 mg tamoxifen (10 mg/ml in peanut oil; Sigma-Aldrich) daily *i.p.* for five days starting at lymphoma manifestation (Martins et al., 2006) (with peanut oil as solvent control), or liposome-encapsulated clodronate, produced as described (Aichele et al., 2003), or empty liposomes as control by intravenous administration (10 µl/g body weight of a 1:1 dilution of a liposome stock adjusted to an OD_{600} [optical density] of 1.2) every 48 hours up to three times, or caffeine (0.4 mg/ml in drinking water; Sigma-Aldrich) starting after weaning (Kramata et al., 2005), or N-acetyl-cysteine (NAC; as a 0.5% solution in drinking water; Hexal) starting at mid-embryonic stage (Reimann et al., 2007), or lisinopril (60 mg/l in drinking water; Sigma-Aldrich) starting at around four weeks of age, with all orally applicable drugs provided *ad libitum*.

Immunoblotting, Immunoprecipitation and Antibody List

Briefly, whole-cell extracts for immunoblotting (IB) were generated by lysing cells in SDS sample buffer (60 mM Tris-HCl at pH 6.8, 10% glycerol, 2% SDS, and 5% 2-mercaptoethanol), and aliquots corresponding to 50-200 µg of protein were resolved on SDS-polyacrylamide gels and transferred to Immobilon P membranes (Millipore). For HA-Suv39h1/Smad IP, 200 µg of protein lysates (produced by lysing cells in 200 mM NaCl, 50 mM Tris, pH 8.0, 5 mM EDTA, 1% Triton-X, 10% glycerol, 1 mM sodium orthovanadate,

2 mM DTT, 1.5 µg/ml aprotinin, 0.3 µg/ml pefabloc and 6 µg/ml leupeptin) were incubated with a 1:40 dilution of anti-HA or IgG-control antibodies at 4°C for 3 hours, and IB was carried out as described (Schmitt et al., 1999), and blots were probed with Smad antibodies. Immunophenotyping by flow cytometry as well as antigen detection by immunofluorescence (IF), immunohistochemistry (IHC), immunoblotting (IB), and immunoprecipitation (IP) was carried out with antibodies against 53BP1 (sc-22760, Santa-Cruz Biotechnology [SCBT], 1:1000 dilution), 53BP1-P-Ser25 (NB 100-2279, Novus Biologicals, 1:1000), Annexin V (no. 556419, BD Pharmigen [BDP], 1:200), ARF (ab80, Abcam, 1:1000), Bcl2 (no. 554087, BDP, 1:2000), ATM (2C1, GeneTex, 1:1000), ATM-P-Ser1987 (no. 4526, Cell Signaling Technology [CST], 1:1000), Bcl6 (594, Dako, 1:25), CD10 (56C6, Novocastra, 1:50), CD68 (PG-M1, Dako, 1:50), cleaved Caspase 3/Asp175 (no. 9661, CST, 1:200), Cyclin A (CY-A1, Sigma, 1:1000), estrogen receptor (sc-542, SCBT, 1:100), F4/80 (BM8, eBioscience, 1:50), hemagglutinin HA.11 (16B12, Covance, 1:1000), H2A.X-P-Ser139 (*i.e.* γ-H2AX) (JBW301, Upstate Biotech, 1:100), H3K4me3 (no. 9751, CST, 1:1000), H3K9ac (no. 9649, CST, 1:1000), H3K9me3 (ab8898, Abcam, 1:1000), H3K27me3 (provided by T.J., 1:1000), H4K20me3 (ab9053, Abcam, 1:1000), HP1γ (no. 07-332, Upstate Biotech, 1:1000), Ki67 (Tec3, Dako, 1:2000, and MIB-1, Dako, 1:2000), Mum1/IRF4 (kindly provided by B. Falini; 1:20), c-Myc (N-262, SCBT, 1:1000), $p15^{INK4b}$ (no. 4822, CST, 1:1000), $p16^{INK4a}$ (M-156 and F-12, SCBT, 1:500 and 1:2000, respectively), $p21^{CIP1}$ (C-19, SCBT, 1:500), p53 (CM5, Novocastra, 1:2000), p53-P-Ser18 (no. 9284, CST, 1:1000), PAI-1 (sc-8979, SCBT, 1:50), Puma (ab9643, Abcam, 1:2000), Rb (G3-245, BDP, 1:100), Smad2-P-Ser465/Ser467 (no. 3108, CST, 1:1000), Smad3-P-Ser423/425/Smad1-P-Ser463/465 (no. 9514, CST, 1:20), Smad4 (no. 9515, CST, 1:1000), TGF-β1 (no. 3709, CST, 1:50), and α-tubulin (T5168, Sigma-Aldrich, 1:8000). Immunophenotyping by flow cytometry was conducted with antibodies against B220 (CD45; RA3-6B2, BDP, 1:200), IgM (no. 553437, BDP, 1:200), Thy1.2 (CD90.2; no. 553003, BDP, 1:100), CD11b (M1/70, BDP, 1:200) and CD206 (clone MR5D3, no. MCA2235A488, AbD Serotec, 1:20). Where required, corresponding peroxidase- and or fluorescence-conjugated secondary antibodies (GE Healthcare, Molecular Probes, SCBT) were used. Staining intensities of Smad3-P or PAI-1 *in situ* were semi-

quantitatively assessed (- *vs.* +, ++ or +++; converted into numeric values 0, 1, 2 or 3 to calculate a mean in some experiments [where a value of around 0.5 would translate into (+)]). TGF-β1 protein concentrations were also measured by ELISA (Quantikine, R&D Systems) in HCl-activated cell-free culture supernatant in accordance with the manufacturer's protocol.

SUPPLEMENTAL REFERENCES

Kagami, S., Border, W. A., Miller, D. E., and Noble, N. A. (1994). Angiotensin II stimulates extracellular matrix protein synthesis through induction of transforming growth factor-beta expression in rat glomerular mesangial cells. J Clin Invest *93*, 2431-2437.

Koca, E., Haznedaroglu, I. C., Uner, A., Sayinalp, N., Saglam, A. E., Goker, H., and Ozcebe, O. I. (2007). Angiotensin-converting enzyme expression of the lymphoma-associated macrophages in the lymph nodes of Hodgkin's disease. J Natl Med Assoc *99*, 1243-1244, 1246-1247.

Mantovani, A., Sozzani, S., Locati, M., Allavena, P., and Sica, A. (2002). Macrophage polarization: tumor-associated macrophages as a paradigm for polarized M2 mononuclear phagocytes. Trends Immunol *23*, 549-555.

Strasser, A., Harris, A. W., Bath, M. L., and Cory, S. (1990). Novel primitive lymphoid tumours induced in transgenic mice by cooperation between myc and bcl-2. Nature *348*, 331-333.